Automated interpretation of ultrasonographic prostate images

A.L. Huynen

AUTOMATED INTERPRETATION OF ULTRASONOGRAPHIC PROSTATE IMAGES

A.L. Huynen

CIP-GEGEVENS KONINKLIJKE BIBLIOTHEEK, DEN HAAG

Huynen, A.L.

Automated interpretation of ultrasonographic prostate images /
A.L. Huynen. [S.l. : s n.]. - Ill
Proefschrift Katholieke Universiteit Nijmegen. - Met lit. opg.
ISBN 90-9008932-2
Trefw.: prostaat / echografie (geneeskunde) / beeldverwerking.

AUTOMATED INTERPRETATION OF ULTRASONOGRAPHIC PROSTATE IMAGES

Een wetenschappelijke proeve op het gebied van de Medische Wetenschappen

Proefschrift

ter verkrijging van de graad van doctor
aan de Katholieke Universiteit Nijmegen,
volgens besluit van het College van Decanen
in het openbaar te verdedigen op vrijdag
29 maart 1996, des namiddags te 1.30 uur precies

door

Anton Leonard Huynen
geboren op 10 mei 1967 te Heerlen

Promotor	Prof.Dr. F.M.J. Debruyne
Co-promotores	Dr.Ir. H. Wijkstra
	Dr. J.J.M.C.H. de la Rosette

Front Cover	A graphic representation of a recursive binairy fractal tree, made by PhoTon Imaging Nijmegen.
Print	CopyPrint 2000, Enschede

This thesis was financially supported by:
Bard Benelux B.V., Bayer B.V., Hoechst Holland N.V.,
Karl Storz Endoscopie Nederland B.V., Lorex Synthélabo B.V.,
Mediteg Diagnostics B.V., Pfizer B.V., Pie Medical Benelux B.V.,
Schering-Plough B.V., Yamanouchi Pharma B.V.

'Even things that are true can be proved'
Oscar Wilde

Contents **Page**

Chapter I
Introduction and Outline - 9 -

Chapter II
Boundary detection - 15 -

Chapter III
Statistical parameters for the classification of image texture and the correlation with histopathology - 25 -

Chapter IV
Implementation of the tissue discrimination algorithms - 37 -

Chapter V
Impact of automated image interpretation on clinical decision making - 51 -

Chapter VI
Multiple histology-class tissue discrimination - 59 -

Chapter VII
Position dependant enhancement of ultrasonographic textural features - 67 -

Chapter VIII
Future developments - 79 -

Chapter IX
Summary and Conclusion - 87 -

References - 97 -

Publications - 105 -

Curriculum vitae - 111 -

Chapter I

INTRODUCTION AND OUTLINE

Introduction

This thesis describes methods for automated interpretation of ultrasonographic prostate images The prostate is a male secretory gland situated in the lower pelvic area The main areas of the prostate are the Central Zone (CZ) and the Periferal Zone (PZ), separated by the Transition Zone (TZ), histologically identical to the PZ. The CZ is the origin of Benign Prostatic Hyperplasia, while Prostate Carcinoma (PCa) is mainly situated in the PZ and TZ (Boyle, 1994). These two diseases are the main medical problems in the prostate and the incidence of both diseases increase with age. The aging of the population, therefore, causes prostatic complaints to become a major problem in clinical health care

For the diagnosis of prostatic complaints with suspicion for prostate carcinoma, mainly three clinical tests are available; the Digital Rectal Examination (DRE), the Prostate Specific Antigen (PSA), and TransRectal UltraSound (TRUS) of the gland DRE is used to assess regularity, firmness, and size of the gland It is easy applicable and an indication about pathology can be obtained. The accuracy of the DRE assessed volume and the sensitivity for cancer detection on rectal examination are low Furthermore, of all cancers detected with DRE, only 33% are organ confined (Faul and Altwein, 1995) The use of PSA as tumour marker has gained increasing interest in recent years, caused by its high sensitivity. However, the method is not tumour specific because PSA is produced by epithelial prostate tissue BPH also produces PSA and an overlap exists between the PSA levels seen for cancer tissue and for BPH, especially for large benign prostates Although more time consuming than DRE, TRUS is also easy applicable and a cheap investigational tool

Imaging of the prostate is important for both BPH and PCa It enables the urologist to investigate the interior and especially the anterior non-palpable parts of the gland With ultrasonographic imaging, an accurate method for volume determination of the gland is available. The volume of the prostate is an important diagnostic factor for the determination of BPH, for the selection of treatment modalities, and for the evaluation of treatment success for this disease. The volume of the gland also facilitates the interpretation of PSA levels for the detection of PCa and the differentiation between BPH and PCa. Furthermore, the internal echodensity and -texture are used to assess the probability of malignancy. Also the symmetry of the gland and the regularity of the capsule are used for the diagnosis of PCa If there is a suspicion for the presence of cancer, TRUS is used to guide tissue puncture biopsies to the image regions with increased probability of malignancy, or 'at random' if the entire gland appears normal in the ultrasound images. Random biopsies are placed regularly in the prostate, to obtain tissue samples from all prostate regions.

Ultrasonography uses soundwaves of high frequencies. The majority of ultrasound transducers used for the visualisation of prostate tissue apply frequencies near 7 5 MHz. First, the echoprobe transmits a soundwave into the medium to be

visualised The particles in the tissue absorb energy from the sound wave and transmit this energy back to the tissue as new, independent soundwaves (Wells, 1977). The part of these secondary soundwaves that is transmitted in the direction of the ultrasound transducer is called the backscattered ultrasound signal. This signal is recorded by the transducer, primarily used to generate the soundwave, and quantified. Because the soundwaves travel through the tissue at a certain speed, the time between the transmittal of the ultrasound and the recording of the reflections is related to the distance between the ultrasound transducer and the reflecting tissue particles. By moving the transducer, a two- (and even three-) dimensional construction of the ultrasound reflections can be made. By transforming the reflection amplitudes to grey values, an ultrasound image is produced.

The dissimilarity in histologic appearance of different tissue types may be reflected in the ultrasonic characteristics. In this way, it may be possible to differentiate tissue based on its ultrasonographic image properties The reflected soundwaves interfere and these interferences form a pattern in the constructed image, called texture The image texture is specific for the number and distribution of the tissue particles reflecting the ultrasound and consequently for the tissue histology. The human perception, however, is not capable to discern all the differences in the image texture The changes in the texture may be too small, or they occur in a domain not used by the human perceptual system to distinguish texture Furthermore, most modern ultrasound equipment displays the images in 256 grey tones (8 bit). The human observer is able to perceive the difference between images with 7 bit and 8 bit grey values in images with smooth grey scales. In ultrasound images, however, no difference is noted between 5 bit or more grey values (unpublished observation). The additional information, provided by the ultrasound equipment by increasing image depth (using more grey values), can not be used by a human interpreter

The sensitivity and specificity of DRE and of TRUS vary considerably between different reports (Clements et al 1991; Lee et al. 1989a; Mettlin et al. 1993; Mettlin, 1993), causing the separate investigators to prefer disparate examination tools. Caused by the lack of accuracy of the diagnostic methods, histopathologic tissue examination is always necessary to confirm the diagnosis. For the guidance of tissue biopsies, patients prefer ultrasound above digital guidance (Aus et al. 1993). However, the first biopsy (series) in the prostate has a high False Negative rate (Keetch et al 1994) and with six regularly placed 'random' biopsies more cancer is detected than with biopsies directed to tissue areas ultrasonically suspected to be malignant (Hodge et al. 1989a) Ultrasound guided but especially random biopsies are shown to detect clinically undiagnosed prostate cancer (Coplen et al. 1991). The role of ultrasound for the detection of prostate carcinoma and its additional value to DRE is unclear. Up to 42% of prostate cancer is reported to be isoechoic but clinically significant (Ellis and Brawer, 1994). These findings were confirmed by Ferguson and co-workers (1995) for PSA detected (DRE negative) carcinoma: no pathologic difference could be found between TRUS + and TRUS- malignant prostate tissue. The

hypothesis that high grade tumours arise from low grade tumours and should be considered as late stages in the development of prostate cancer does not hold true (Epstein et al. 1994) If PCa is diagnosed and untreated, it progresses slowly but relentlessly, even in its early stages (Scardino, 1989). Therefore, early detection of PCa is of utmost importance, especially for cancer not ultrasonically detectable

Like the interpretation of many imaging modalities, the deciphering of the information in TRUS images improves with training (Hill et al. 1991). The use of image interpretation in the clinical diagnostic process is subjective and irreproducible. To improve the diagnosis of prostate complaints, we automated the interpretation of TransRectal UltraSound images of the prostate. With improved accuracy and reproducibility of TRUS in the clinical decision process, the task of the diagnostician will be simplified and patient care will improve.

Outline

This introductory chapter described the human prostate and the ultrasound imaging, used to visualise the gland. Caused by drawbacks of the human perception, not all information in the ultrasound images can be retrieved. With specific algorithms, this information can be used directly by a computer system, or transformed to a more perceptible domain for human interpretation. This thesis describes automated algorithms to facilitate and improve the interpretation of ultrasonographic prostate images. The two major applications of ultrasound for prostatism diagnosis and follow up are automated: volume determination of, and tissue discrimination in the prostate

Because the tissue discrimination algorithms are trained with the images of puncture biopsies from prostate tissue, the assessment of tissue histology is only valid for prostate tissue The tissue discrimination algorithms must, therefore, be limited to the prostate region. In Chapter II, an edge detection algorithm is presented for the determination of the prostate boundary With a low-pass filter, the edge-detection disturbing speckle is reduced. Applying minimum and maximum filters, the second derivative is approximated and used to detect all edges in the image. Using knowledge based ultrasound features of the gland, the relevant edges are selected and interpolated to form a closed contour, displaying the prostate boundary. With this boundary, the image is segmented into a prostate region and a non-prostate region. The area in the image occupied by the prostate is determined, to restrict the region to be analyzed by the tissue discrimination algorithms. By calculating this image area for consecutive cross-sections and by summation and multiplication with the inter-image distance, also the volume of the gland can be calculated.

The most important purpose of ultrasound in the detection of prostate carcinoma is the differentiation of visualised tissue. Because pathology of the tissue may be reflected in the ultrasonographic image texture, texture quantifying parameters are used for this application. In Chapter III, the image processing parameters for texture

quantification are described. The parameters calculated from the images form multi-dimensional feature vectors, which are labelled with the histology of the corresponding tissue. A classification process, which divides the group of vectors, corresponding to the histology labels, by looking only at the image parameters, is able to predict the tissue histology for a sample, if only the image processing parameters are known. In this way, assumptions about the prostate tissue histology can be made, by analyzing the ultrasound images. The second part of this chapter describes a non-parametric classification algorithm. Using the mutual information, the decision with the maximum local information about the classification process is selected and the classification is split up into two smaller decision problems. Each sub-problem is treated the same way, successively deviding the decision problem into (smaller) subproblems. A decision tree is built, with the internal nodes representing the decisions and the external nodes corresponding to the class assignments of the samples. In every external node, the samples reaching that node are classified according to the most appropriate histology.

In Chapter IV, the implementation of the tissue discrimination algorithms is reported, as well as the use of the system during the training phase and in daily clinical practice. Using the ultrasound images of puncture biopsies, a decision tree is constructed representing the obtained information about the correlation between image texture and tissue histology. With this decision tree the images of prostates with unknown histology are classified and the tissue histology is predicted for small regions in the image. According to the predicted probability of malignancy, the regions are colour-coded. With a sliding window for the colour-coding, the entire prostate region can be analysed and the assessment of tissue histology in, and the interpretation of the ultrasound images is facilitated.

The images of puncture biopsies represent only a limited part of all patients visiting the outpatient clinic with prostatism complaints; the patients with clinical positive test outcome. The classification results in this biased population are not valid for the total patient population, caused by the dissimilar incidence of prostate carcinoma for these two populations. To examine the value of computerized tissue discrimination, the results of the automated algorithm are prospectively compared with the clinical diagnostic factors in Chapter V. Using the biopsy rate and the rate of incidental carcinoma, the classification results for the total patient population with prostatism complaints are calculated. In this way, a true prospective comparison can be done and the benefit of automated texture interpretation during everyday clinical practice can be assessed.

The initial classification algorithm was designed as a two class decision method for the discrimination between benign and malignant prostate tissue. Only the tissue biopsies with these two histologies were included during the training phase. During prostate investigations, however, other tissue types are also seen. The main additional tissue type is prostatitis (prostate inflammation). To investigate the

influence of prostatitis samples on the tissue discrimination results, the classification algorithms were extended in Chapter VI to be able to discriminate more histology classes The combination of prostatitis samples with benign samples, to represent non-malignant tissue, as well as the combination of prostatitis with malignant samples, to form the biopsy samples with deviations from benign tissue, were examined. Also the classification of the three histology classes simultaneously was investigated.

The use of ultrasound for visualisation and automated interpretation has the disadvantage that the physics of ultrasound produce inhomogeneous images. The textural descriptions are not only depending on the ultrasound characteristics of the visualised material, in our case prostate tissue, but also on the position in the image where this material is visualised. In Chapter VII, two correction algorithms are described to overcome the disadvantages of the inhomogeneity of the textural parameters A pre-processing step is introduced to eliminate image-angle dependencies, caused by the use of a rotating single-element ultrasound transducer A post processing (correction) algorithm is described to adjust for dependency of the parameters to the distance to the ultrasound probe, caused by interference patterns and attenuation of the ultrasound signal

In Chapter VIII, a short description is given of the ongoing research. Furthermore, a 3-dimensional presentation of the prostate is given by combination of the contours in consecutive cross-sections. The improvement of the classification results of the tissue discrimination algorithms by incorporating the clinical diagnostic factors is demonstrated Finally, some ideas for the improvement of the colour-coding and of the combination of the segmentation and tissue discrimination algorithms are given

In the last chapter, this thesis is summarised and the conclusions are presented Because this thesis is not a collection of single papers, the referenced literature is listed at the end of the thesis, instead of at the end of each chapter.

The edge detection algorithm for the segmentation of the images was selected from literature. Its implementation and evaluation, during prostate volume measurements, and the interpolation to form the prostate contour, were examined by R G. Aarnink. The description of the co-occurrence matrix, the statistical parameters, and the original binairy decision tree are all extracted from literature. For explanatory reasons and to give a complete description of the algorithms, these methods are also reported in this thesis The applicability of the co-occurrence parameters for the discrimination of prostate tissue was tested during a pilot study in close cooperation with R.J.B. Giesen This cooperation resulted also in the selection of a decision tree as classification algorithm The theoretical analysis of the decision trees, as described in the 2nd part of Chapter III, and all following chapters, is original work performed by the author.

Chapter II

BOUNDARY DETECTION†

† Methods based on : 'A practical clinical method for contour determination in ultrasonographic prostate images'
R.G. Aarnink, R.J.B. Giesen, A.L. Huynen, J.J.M.C.H. de la Rosette, F.M.J. Debruyne and H. Wijkstra.
Ultrasound in Medicine & Biology, Vol. 20:p.p. 705-717, 1994.

Abstract

This chapter describes a method for the segmentation of an ultrasound image into a prostate and a non-prostate region. With linear filters, all possible edges in the image are detected. Using knowledge based features of the shape and ultrasonic appearance of the gland, the correct edges are amplified and selected Next, the gaps between the selected edges are interpolated to form the prostate contour.

Introduction

This thesis presents methods for the automated interpretation of ultrasonographic prostate images. The prostate boundary is a very important parameter for the interpretation of these images and the detection of prostate carcinoma By looking at the contour of the gland in transverse images, information can be obtained about the regularity and symmetry of the gland and of capsular penetration or extension of malignancy beyond the prostate capsule. Also for automated tissue discrimination algorithms, the segmentation of the image into prostate and non-prostate regions is very important The tissue discrimination algorithms in this thesis are trained with the images from puncture biopsies. These puncture biopsies only represent (benign as well as malignant) prostate tissue and, therefore, the results are only valid for the prostate region of the ultrasound images. A prostate image, however, displays not only the gland but also the peri-prostatic area of the lower abdomen. To analyse the image only at the valid regions, it has to be segmented into a prostate and a non-prostate region. The restriction of the region of analysis to the prostate area has the advantage that the calculations will be performed quicker. Furthermore, because the peri-prostatic area is not analyzed, it will not influence the interpretation of the ultrasound appearance of the prostate tissue.

For automated contour detection in ultrasonic prostate images, few methods have been described in literature Contour detection algorithms frequently used in echo-cardiography, can not be used because of the computational load, the need for human interaction, the use of stereo vision or motion in time, the lack of use of global information, and the poor performance rates for images with low Signal to Noise Ratio One method developed at our clinic used pre-defined prostate contours, fitted on a number of contour points (Hendrikx et al. 1989). This method, however, is not practically applicable, because of the need for human interaction for the determination of the contour points and the time consumption of the fitting process. Prater and Richard (1992) described a method to segment ultrasonic prostate images using feed forward neural networks. The disadvantage of this technique is the large interaction needed for each series of images. An expert sonographer will have to segment one or more of the images for each prostate, in order to be used as training set of the network. The training of the network, necessary for each series of images, takes approximately 1 hour and segmentation takes 9 minutes per image. Furthermore, this

technique is sensitive to texture changes caused by, for instance, carcinoma and does not deliver a single, connected prostate region after segmentation.

Material and Methods

In our application, differentiations of the grey levels in the images are used. Edges in images are relatively high frequency phenomena according to the surrounding non-edge image parts. Therefore, a filter which amplifies the high frequencies, like the Laplace operator (second derivative), can be used to detect and locate these edges. The first derivative of the image is a measure for the strength of the edges A combination of the first and the second derivative gives an edge intensity image, in which edges are located and quantified. This edge intensity image on its turn can be used as a base for the prostate boundary determination. Inside the computer, the images are represented as a two-dimensional collection of grey values. Therefore, the derivatives of images can be calculated by numerical approximation of the image surface. The use of derivatives of the grey value images has one drawback: the extreme sensitivity to high frequency components as noise and speckle. For edge detection in ultrasonic images, the Laplacian edge operator has to be combined with a low pass pre-filter, to circumvent the sensitivity for noise and speckle structure. A frequently used combination is the use of a Gaussian pre-filter, known as the LoG filter (Laplace of Gaussian), and is extensively described and evaluated by van Vliet and co-workers (1989) The described combination of the gradient and the Laplace of the image is a compromise between accuracy and computation time.

The contour determination consists of four parts; edge detection, edge enhancement, edge selection, and edge linking. The images are compressed in the space domain, to reduce the computation time. Two differentiations of these compressed images are used· the second derivative, with a zero crossing detector to locate the edges, and the gradient image, used for calculation of the strength of the edges. These two derivatives are combined to yield the edge intensity image, used for the enhancement, selection, and linking. To reduce the sensitivity to noise and speckle patterns, a low-pass pre-filter has to be applied A Gauss-filter will perform better, but a uniform blur will be quicker. With very small Signal To Noise Ratios, the filter size will have to be very large. Because a uniform blur filter can be implemented by a linear filter in one direction, followed by the same filter in the direction perpendicular to the first one, this filtering technique is much faster than a Gauss filter. Because linear filters can be implemented with a sliding window technique, the computation time is almost independent of the used filter size. Therefore, the use of large filter sizes, as needed for ultrasonic images, does not involve a major time consumption. The size of the filters, however, is not only dependent on the SNR in the images A compromise has to be found with the edge displacement, which is related to the filter-size. In our application, a blur filter size of 21 by 21 pixels is a good compromise between the displacement of the edges and the detection of noisy

edges not contributing to the prostate contour. After filtering, the images are compressed in both x and y direction by a factor 3. This will speed up the rest of the calculations by approximately 9 times.

For explanatory reasons, a one-dimensional representation of the method is given in Figure 1a to Figure 1h. Figure 1a presents the grey value of a signal containing an edge. According to the Marr-Hildreth operation, the Laplace is approximated with the Second Derivative in Gradient Direction (SDGD). This operator computes the second derivative in the direction of the local gradient and in this way adapts itself perpendicular to the local edge direction. In our algorithm, the SDGD is implemented with local minima (Figure 1b) and maxima (Figure 1c) filters, combined with the grey value to assess the local gradient in the direction from the minimum (Figure 1d) and to the maximum (Figure 1e):

$$SDGD_n(x,y) = GradMax_n(x,y) - GradMin_n(x,y)$$
$$GradMax_n(x,y) = Max_n(x,y) - Grey(x,y)$$
$$GradMin_n(x,y) = Grey(x,y) - Min_n(x,y)$$

GradMax,Gradmin: *the gradient in the direction of the maximum resp. from the minimum*
Max_n, Min_n: *the maximum and minimum in a neighbourhood n*
Grey: *the grey value*

In this method two parameters can be adjusted for the detection of specific edges: the filter size n for the various filters and the effective shape of the filters. The ideal filter size n is related to the size of the features to be detected (edges) and the accuracy of this detection. In our case, visual comparison lead to the use of a filter size of 8 by 8 pixels in the compressed images. Ideally, the shape of the filters has to be circular to prevent directional preferences, but no difference could be indicated with the use of square filters. Therefore, it seems plausible to use square shapes for the determination of the minimum and maximum filters, which provides an easy and fast way to implement the SDGD filtering technique.

After calculation of the Second Derivative image (Figure 1f), zero crossings in this image have to be detected for the localization of the edges (Figure 1g). For the detection of zero crossings in the two-dimensional plane, a one-dimensional zero crossing detector is applied:

$$(G_x = 0 \wedge G_{x-1}G_{x+1} < 0) \vee$$
$$(G_xG_{x-1} < 0 \wedge |G_x| < |G_{x-1}|) \vee$$
$$(G_xG_{x+1} < 0 \wedge |G_x| \leq |G_{x+1}|)$$

G_x: *the SDGD value at position x*

The zero crossing detector marks the edge pixel with non-negative grey value as the boundary pixel. The one dimensional zero crossing detector is applied horizontally, vertically, and diagonally and the four results are combined with a logically OR operator:

$$ZeroCrossing = ZC_{-} \vee ZC_{\setminus} \vee ZC_{|} \vee ZC_{/}$$

ZC_v: *the one-dimensional zero crossing in direction v*

The calculated zero crossing is used as a mask for the edge strength in the images (Figure 1h) The edge strength is calculated using the 'Blur Minimum Morphological Edge Detector' (Lee et al. 1987). This operator uses the local gradient images as calculated for the SDGD

$$EdgeStrength = MIN(GradMin, GradMax)$$

The combination of the edge strength operator with the zero crossing in the SDGD image yields the Edge-Intensity image, in which the edges are located as well as quantified This final edge intensity image contains edges that form closed loops in the image, or lines terminated at the borders of the image. Ideally, the contour of the prostate would be one closed edge Practically, however, the contour is formed by parts of a number of edges (see Figure 2h). The correct parts have to be selected and interpolation is necessary to fill the gaps between these partial contours

Before the selection of the edges takes place, first an edge enhancement operation is performed. Normally, edge enhancement takes place by applying a threshold procedure, which actually is a pre-selection procedure. A disadvantage of global thresholding is the non-selectivity of the approach and, therefore, the possible loss of correct edges (contour parts) A more sophisticated way is to apply a threshold with hysteresis. The detected edges form closed contours and the threshold with hysteresis tends to keep long lines or closed curves unbroken First a high threshold is used to select initial edges points. Then, all points connected to edge points and exceeding a low threshold are also marked as edge points. This step is repeated (with constant low threshold) until no further points can be marked as belonging to the contour For the edge selection, feature knowledge of the object to be detected can be used. In the case of the prostate, the expected shape and grey value appearance are used The gland is represented hypo-echoic according to the peri-prostatic fat, surrounding the glandular tissue. Looking from within the gland, the edges to be detected, are transitions from dark to light. Therefore, edges from light to dark can be deleted. For this step, the mid of the prostate has to be pointed out, in the central cross-section, by human interaction After removal of light-to-dark transitions, the edges forming the prostate boundary have to be selected. The shape of the prostate is expected to be kidney-like. Therefore, the search procedure for the initial edge points will conduct a radial search in the upper part of the image and a linear search

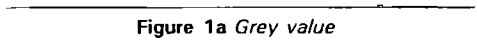

Figure 1a *Grey value*

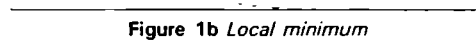

Figure 1b *Local minimum*

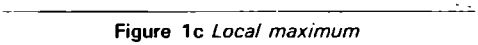

Figure 1c *Local maximum*

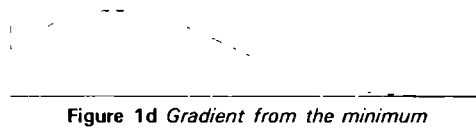

Figure 1d *Gradient from the minimum*

Figure 1e *Gradient to the maximum*

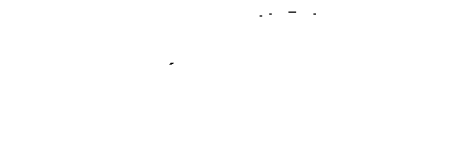

Figure 1f *2nd Deriv. in Gradient Direction*

Figure 1g *Zero crossing in SDGD signal*

Figure 1h *Edge strength*

for the lower part of the image. The radial search selects edge-points at evenly distributed directions, while the linear search selects these points in evenly spaced colums. Points whose distance to the mid of the gland is not within the expected range, or whose position is too different from its neighbours are removed. Using the selected points, the edges found in the image are followed to get the contour pixels. The detected edges will have to be linked to fill in gaps, where the contour is not detected. Small gaps are filled with linear interpolation of the pixels on the found edges and larger gaps with quadratic (parabolic) interpolation, using the endpoint of one of the edges as third point for interpolation.

Results

Figure 2a to Figure 2l present an example of the contour detection in an ultrasonographic prostate image. Figure 2g, however, contains only negative, zero, and positive regions, coloured as black, grey, and white, the states needed for the zero crossing detection, with no further differentiation. The calculation of the contour in this image took about 18 seconds (using a 486DX2 50 MHz personal computer).

As can be seen from the example, the automatically detected contour segments the image reasonably accurate into a prostate and a non-prostate region To evaluate its accuracy, the contour determination was also used for the calculation of the prostate volume (Aarnink et al 1995). The area of the image consisting of prostate tissue was computed by counting the number of pixels within the contour. This area was determined in every image of a series of transverse cross-sections. All these areas were added and multiplied with the distance between the images to calculate the volume of the prostate. Compared to volume determination used in daily urological practice, this automated volume is much more accurate.

Discussion

With the automated detection and presentation of the prostate boundary in the ultrasound images, the interpretation of the regularity of the capsule and the symmetry of the gland is simplified. With Artificial Intelligence, the interpretation itself may be automated by definition and quantification of parameters describing the regularity and symmetry. Also the combination of segmentation information and textural analysis may be used to improve the interpretation of the images and the detection of pathologic tissue (see Future Developments).

A disadvantage of the method is its dependence on the image quality and its sensitivity to high contrast artifacts as cysts, calcification or shadows. This disadvantage, however, is partly overcome by the search algorithm for the edge detection. The distance of the contour points to the mid and the continuity of this distance do not allow abrupt changes in the direction of the contour.

Another disadvantage is the compression of the image in the space domain. This compression speeds up the calculations approximately nine times, but also introduces contour displacement of one-and-a-half pixel on the average. For the volume determination, the displacements of the different contour parts will eliminate each other For the tissue discrimination algorithms, this displacement is negligible, due to the relative large calculation windows.

The tissue discrimination algorithms, described in this thesis, are trained with longitudinal ultrasound images from puncture biopsies. The segmentation algorithm,

Figure 2a *the original ultrasound image.*

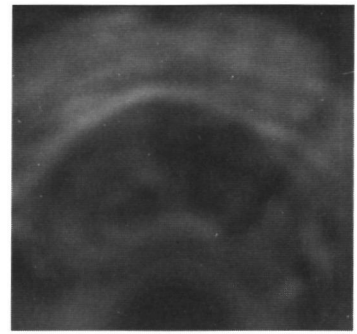

Figure 2b *The blurred and compressed image.*

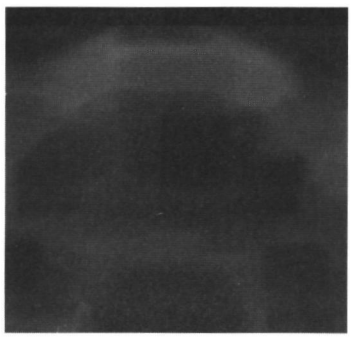

Figure 2c *The local minimum of the image.*

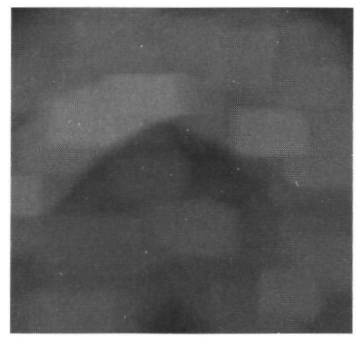

Figure 2d *The local maximum.*

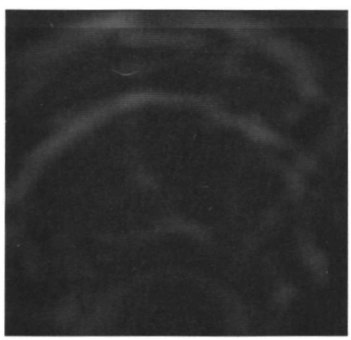

Figure 2e *The gradient in the direction from the minimum.*

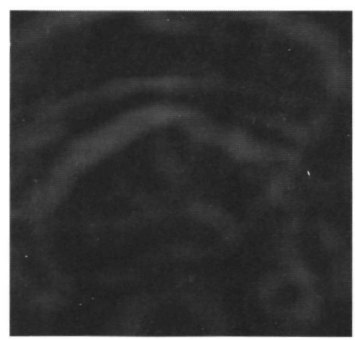

Figure 2f *The gradient in the direction of the maximum.*

Figure 2g *The Second Derivative in Gradient Direction.*

Figure 2h *The zero crossings in the second derivative.*

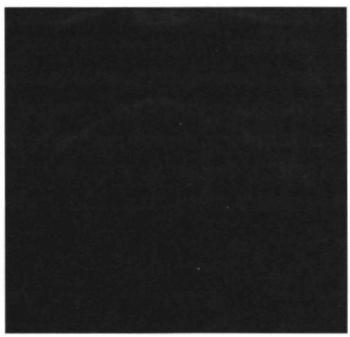

Figure 2i *The edge strength.*

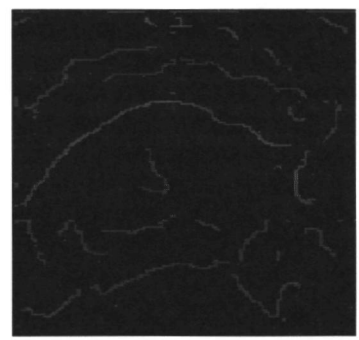

Figure 2j *The edge strength masked by the zero crossings.*

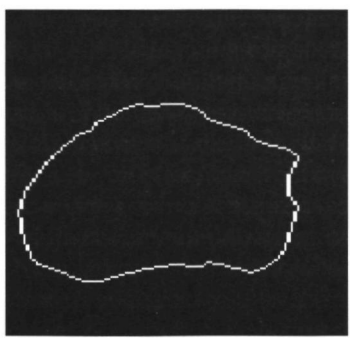

Figure 2k *The selected contour.*

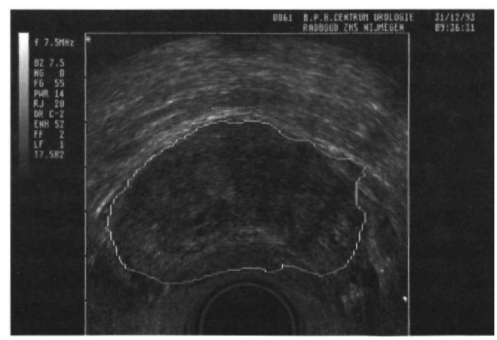

Figure 2l *the ultrasound image with the projected contour.*

however, was developed for volume calculation and, therefore, only suitable for transverse images. The tissue discrimination algorithms are also valid for transverse images (Giesen et al. 1995a; 1995b) and in these images the segmentation can be used to restrict the region of interest

Conclusion

With the automated segmentation of ultrasonographic images into prostate and non-prostate regions, the Region Of Interest for the tissue discrimination algorithms can be reduced to the prostate region. By performing the segmentation in consecutive cross-sections and calculating the area of the prostate region in every image, the volume of the gland is calculated by summation and multiplication with the inter-image distance. Automated volume calculation simplifies the ultrasonographic prostate examination and reduces the necessary investigation time.

Chapter III

STATISTICAL PARAMETERS FOR THE CLASSIFICATION OF IMAGE TEXTURE AND THE CORRELATION WITH HISTOPATHOLOGY

Abstract

This chapter describes image processing parameters, used to quantify the texture of an ultrasonographic image region. The used statistical parameters are based on the co-occurrence matrix, a representation of the joint probability of grey values for neighbouring pixels of the image. The samples of parameters calculated from images of puncture biopsies are classified to examine the relation between the parameters and the histology of the corresponding removed tissue. This classification is done with a binary decision tree, based upon the concept of mutual information. A (nearly) optimal combination of image processing parameters is obtained to represent the histology of the tissue, visible in the image.

Statistical image processing parameters

Introduction

For the automated interpretation of images, features of the images have to be detected and quantified. Three categories of feature extraction are frequently used: spectral, structural, and statistical. The spectral analysis transforms the image from the space domain to the frequency domain and the transformed signal is processed and analyzed and eventually converted back to the space domain. The structural approach uses known or semi-known structures in the image or features of the image It is used to interpret contextual information like shape, regularity, and position of detected objects in the image. We used the structural analysis to determine the zoom factor in the images and to locate the area displaying the ultrasound signal. For example, the zoom factor is represented in the image by marks at the image boundaries, with an intermediate distance of 1 cm. By looking for these marks and counting the number of pixels between them, the zoom factor in the image can be determined. The segmentation of the images into a prostate and a non-prostate region is another example of structural analysis The statistical approach to texture is concerned with the spatial distribution and spatial dependence among the grey tones in a local area. It examines grey value statistics in (parts of) the image Statistics of the n^{th} order use the grey value properties of n pixels simultaneously. Grey level histogram and mean grey value are examples of 1^{st} order statistics. Because 2^{nd} order statistics are used by a human observer for the perception and interpretation of image texture, we used this kind of image processing for the automated interpretation of the images.

Methods

Conners and Harlow (1980) compared the grey level dependence (co-occurrence) method, with grey level run length, grey level difference, and power spectral

methods, for the discrimination between image textures. For these generated textures, the co-occurrence matrixe yielded the best results. Therefore, in a pilot study we tested the use of the co-occurrence matrix for the discrimination between benign and malignant prostate tissue (Giesen and Huynen, 1991). Haralick et al. (1973) described the co-occurrence matrix, in which the 2nd order statistics of the grey values of two neighbouring pixels are described The co-occurrence matrix can be calculated in the following way:

Suppose the area to be analyzed for texture is rectangular and has N_c resolution cells in the horizontal direction (columns), N_r resolution cells in the vertical direction (rows), and that the grey tone appearing in each resolution cell is quantified to N_g grey levels. Let $L_c = (1,2,..,N_c)$ be the horizontal spatial domain, $L_r = (1,2,..,N_r)$ be the vertical spatial domain, and $G = (1,2,..,N_g)$ be the set of N_g quantified grey tones. The set $L_r \times L_c$ is the set of resolution cells of the image ordered by their row-column designations. The image I can be represented as a function which assigns some grey tone in G to each resolution cell or pair of coordinates in $L_r \times L_c$:

$$I: L_r \times L_c \rightarrow G.$$

The grey tone co-occurrence can be specified in a matrix of relative frequencies p_{ij} with which two neighbouring resolution cells occur in the image, one with grey tone i and the other with grey tone j. Considering the matrices of spatial grey tone dependence frequencies as a function of the angular relationship Θ between the neighbouring resolution cells as well as a function of the distance d between them, the matrices can be denoted as $\Phi(d,\Theta)$. This can be done for eight different directions: $(\Theta = n*45° \mid n \in (0..7))$. The probabilities $p(i,j,d,\Theta)$ at row i and column j in these matrices $\Phi(d,\Theta)$ can be calculated from the absolute frequencies $P(i,j,d,\Theta)$:

$$p(i,j,d,\Theta) = P(i,j,d,\Theta) / P(d,\Theta)$$

$$P(i,j,d,\Theta) = \#[\ ((k,l),(m,n)) \in (L_c \times L_r) \times (L_c \times L_r) \mid k-m = COS(\Theta)d,\ l-m = SIN(\Theta)d,\ I(k,l) = i,\ I(m,n) = j\ ]$$

or: the number of pixel pairs in the image with grey value i and j, related by the angle Θ and the distance d.

$$P(d,\Theta) = \Sigma_i \Sigma_j P(i,j,d,\Theta)$$

or: the total number of pixel pairs related by d and Θ

Such co-occurrence matrices of spatial grey tone dependence can be symmetric or a-symmetric, depending on the way of calculating them. By looking only at the absolute value of the distance, the result will be a symmetric matrix $S(d,\Theta)$.

$$S(d,\Theta) = \tfrac{1}{2}\,(\Phi(d,\Theta) + \Phi(d,\Theta + 180°))$$
$$= \tfrac{1}{2}\,(\Phi(d,\Theta) + \Phi^t(d,\Theta)),\ \text{with } \Theta \in (0°, 45°, 90°, 135°)$$

These symmetric matrices were used in our research. For the clinical application, the settings for the calculation of the co-occurrence matrices, yielding the optimal discrimination between benign and malignant tissue, were determined. The optimal values for this classification are: distance $d=3$, $\#_{angles}=2$ ($\Theta \in [0°, 90°]$), and $N_c=30$, $N_r=45$ (resulting in a Region Of Interest of $5x5mm^2$).

The combination of the five co-occurrence parameters Contrast, Entropy, Correlation, Uniformity, and Inverse Difference Moment yielded the best classification results in the research of Conners and Harlow and were tested during the pilot study. These parameters are described by the next calculations performed on the probabilities $p(i,j,d,\Theta)$ (noted as $p(i,j)$) from the co-occurrence matrix $S(d,\Theta)$:

$$Uniformity = \sum_i \sum_j p(i,j)^2$$

$$Contrast = \sum_{n=0}^{N_g-1} n^2 \sum_i \sum_{\substack{j \\ |i-j|=n}} p(i,j)$$

$$InverseDifferenceMoment = \sum_i \sum_j \frac{1}{1+(i-j)^2} p(i,j)$$

$$Entropy = -\sum_i \sum_j p(i,j) \log(p(i,j))$$

$$Correlation = \frac{\sum_i \sum_j ij\,p(i,j) - \mu_x \mu_y}{\sigma_x \sigma_y}$$

with:

$$\mu_x = \sum_i i \sum_j p(i,j)$$

$$\mu_y = \sum_j j \sum_i p(i,j)$$

$$\sigma_x = \sqrt{\sum_i (i-\mu_x)^2 \sum_j p(i,j)}$$

$$\sigma_y = \sqrt{\sum_j (j-\mu_y)^2 \sum_i p(i,j)}$$

During the pilot study, only a small number of samples was evaluated. Furthermore, this study was done with an ultrasound device displaying only 32 grey values and only ultrasonographic suspected lesions were used. With a larger set of tissue samples, from ultrasonographic suspected as well as normal appearing images, and the images recorded with 256 grey values, the Correlation had no discriminating power for the histologic tissue classification The Signal to Noise Ratio (SNR, calculated as μ/σ of the grey value), on the other hand, did have discriminating power and in further research this parameter was used instead of the Correlation.

Decision trees

Introduction

For the classification of prostate tissue, the inter-relation of the histology of puncture biopsy tissue and the texture quantifying image processing parameters at the biopsy location in the corresponding ultrasound image, was determined. In a classification problem, the objects to categorize are, usually, described by a number of calculated features or properties, forming a feature vector. The set consisting of the vectors of all objects, form a multi-dimensional space constituted by the calculated properties. Each property can be represented by a value on one of the axes of the feature space and the classification problem is really the segmentation of this feature space. After segmentation, the feature space consists of several regions, each representing one of the classes of the classification problem. In our case, the feature space was formed by the image processing parameters calculated from ultrasound images and the classification problem is the determination of the histology of the corresponding tissue. Using five texture describing parameters and two histology types, we got a 2-class decision problem in a 5-dimensional feature space.

Parametric as well as non-parametric segmentation techniques can be used. Parametric applications have the disadvantage that knowledge of the segmentation problem has to be used. This knowledge, however, can lead to better classification results, but is usually not available and, therefore, based on assumptions. Examples of parametric classification methods are Bayes' decision rule and discriminant analysis. The advantage of a non-parametric classification algorithm is the ability to segment the feature space without any knowledge of the categorization problem Examples are the k-Nearest Neighbourhood (k-NN), Neural Networks (NN) or Neural Network Simulations (NNS), and decision trees. The disadvantage of the k-NN and NN(S) methods is the determination of the parameters to use for the segmentation technique, e.g the number of neighbours for the k-nearest neighbourhood, or the number of network layers or of neurons per layer for neural network applications For a k-NN classifier, also the scaling of the feature space is a problem, because the distance in this space, used to define the nearest neighbours, is dependant on the scaling. Using a decision tree, the size and structure of the tree 'automatically' adapts

to the decision problem and to the learning set. The scaling of the parameter space is not important, because only one parameter will be used in each decision step. We compared NNS and k-NN classifiers to a decision tree algorithm and found the results of the decision tree to be superior to the other classifier designs (unpublished research) The decision tree method has the attendant advantage, that the algorithm can stay the same for related but different classification problems, while other classification algorithms will have to be tuned or completely altered for the different tasks. NN(S)-applications, for instance, usually have the same number of output 'neurons', as the number of individual classes. It is clear that the complete structure of such a network will have to be changed for different classification problems, e g the classification of prostatitis (inflamed prostate tissue) (de la Rosette et al. 1995) or of more histology types. A decision tree also will have to be altered for the different decision tasks, but in contrast with the other classifier designs, this alteration needs no interaction or supervision from the human observer. The tree construction algorithm will stay the same and only the resulting decision tree will change for different classification problems Another advantage of the use of a decision tree is the ability to calculate the conditional class probabilities of all classes for a sample. These probabilities are equal to the relative frequencies of the different classes, in the external node (see below) reached by the sample This enables us to calculate the probability of malignancy, instead of only assigning the class 'benign' or 'malignant'.

Methods

A decision tree is a collection of internal and external nodes In the internal nodes a split into sub-trees (branches) is made based upon the decision in that node. In our application, a decision is based on the comparison of a parameter value to a corresponding threshold Because there are two outcomes of this comparison ('equal to' and 'larger than' are used together) the decision tree is called binary. The possible thresholds are determined as the average of two consecutive parameter values, from samples with different histology types, in the training data set. When splitting a node, all samples with a parameter value higher than or equal to the threshold are put into the right sub-tree and for all samples with parameter values below the threshold the left sub-tree is chosen. This yields two sub-trees for every internal node.

An important advantage of decision tree classifiers is the classification accuracy (Park and Sklansky, 1990). The features best suited for the classification problem are used in the first part of the decision procedure. These decisions limit the two regions in the feature space occupied by the two consecutive subsets of samples. Because the features with only limited information for the decision process are used at a rather late stage of the decision process, they are only valid for a small region of the feature space. In this way, the influence of redundant or garbage features, which possibly

reduce the classification results, is confined by the more powerful classification features.

This advantage, however, also implies one of the major disadvantages of a tree classifier design: for a global optimal combination of decisions, only exhaustive testing can be used. Of all possible decision trees for a classification problem, the one best suited should be chosen. Therefore, all permutations of all internal nodes have to be tested. Unfortunately, even with a very small number of features (parameters) and a very simple classification problem, the number of possible decision trees grows extremely fast. A decision problem, with n parameters having only two possible values (high/low, on/off) will have T_n^x numbers of possible decision trees with maximal x levels (the maximum number of decisions per sample, $x \leq n$):

$$T_n^x = \sum_{i=0}^{x} E_n^i, \text{ with } E_n^i \text{ the tree with exact } i \text{ levels}$$

$$E_n^0 = 1$$

$$E_n^i = n(2E_{n-1}^{i-1} \sum_{j=0}^{i-1} E_{n-1}^j - (E_{n-1}^{i-1})^2), \text{ and}$$

$$T_0^0 = E_0^0 = 1$$

$$T_n^n = n(T_{n-1}^{n-1})^2 + T_0^0$$

$\#_{Parameters}$	$\#_{Trees}$
0	1
1	2
2	9
3	244
4	238,145

Table I *The number of possible decision trees.*

As can be seen in Table I, the number of trees grows extremely fast when increasing the number of parameters. With parameter values in a continuous range, or with a higher number of possible thresholds in the parameter values, this exponential growth will even be larger. Clearly, this number of possibilities is to large for an exhaustive search. Therefore, in a practical application, decision trees cannot be optimized globally and, consequently, tree construction algorithms rely on local optimization. In every internal node, the optimal decision at that point is made, probably yielding a global, nearly optimal classification. Sethi and Sarvarayudu (1982) presented the use of the Mutual Information as the criterion to select the best split out of all possible splits in the internal nodes of a decision tree:

Suppose the classification problem with X a set of events $x_i \in X$ and C the set of classes $c_j \in C$. The information $I(x_i)$ related to an event x_i, is given by:

$$I(x_i) = -\log_2 p(x_i).$$

The information given by the set X is the expectation of $I(x_i)$:

$$I(X) = \Sigma_i I(x_i)p(x_i) = -\Sigma_i p(x_i) \log_2 p(x_i).$$

The Mutual Information $I(C;X)$ is given by the difference between $I(C)$ and $I(C|X)$. This means the loss of information provided by the knowledge of class $c_j \in C$, if you already know event $x_i \in X$. This is the information gain over the classes C that an event in X presents:

$$\begin{aligned} I(C;X) &= I(C) - I(C|X) \\ &= I(C) - \Sigma_i p(x_i)I(C|x_i) \\ &= I(C) + \Sigma_i p(x_i)(\Sigma_j p(c_j|x_i) \log_2[p(c_j|x_i)]) \\ &= I(C) + \Sigma_i\Sigma_j p(x_i)p(c_j|x_i) \log_2[p(c_j|x_i)] \\ &= -\Sigma_j p(c_j) \log_2[p(c_j)] + \Sigma_i\Sigma_j p(x_i)p(c_j|x_i) \log_2[p(c_j|x_i)] \\ &= -\Sigma_i\Sigma_j p(c_j,x_i) \log_2[p(c_j)] + \Sigma_i\Sigma_j p(c_j,x_i) \log_2[p(c_j|x_i)] \\ &= \Sigma_i\Sigma_j p(c_j,x_i) [-\log_2[p(c_j)] + \log_2[p(c_j|x_i)]] \\ &= \Sigma_i\Sigma_j p(c_j,x_i) \log_2[p(c_j|x_i)/p(c_j)] \end{aligned}$$

The Mutual Information is maximal if $I(C|X)$ equals zero. The Mutual Information about the classification problem C, provided by event X $I(C;X)$, equals the information provided by the knowledge of the class membership $I(C)$. No further information is gained by knowledge of the class membership after the event x is known. This means that the set of events X, purely separates all classes in C. In a two class decision problem with a binary tree, $1 \le i \le 2$, $1 \le j \le 2$. In our case, the event x_1 represents the parameter value to be below the threshold and x_2 is equal to a parameter value equal to, or above the threshold, c_1 represents benign tissue and c_2 represents malignant tissue.

Because the Mutual Information, for class c_j, is related to the a priori probability $p(c_j)$, the information gain for classes with small or large priors is low. Consequently, the use of the mutual information in a classifier design, leads to misclassification errors, related to the difference in the a priori probabilities of the classes c_j. With very unbalanced priors, as in a cancer detection program, this leads to very low sensitivity. To avoid these misclassification errors, all classes were weighted, to equal the a priori probabilities. As the a priori probabilities of the classes are not known, an estimation is made on the relative frequencies in the training data set.

For the determination of the best split in a node, the mutual information of all possible thresholds over all parameters was calculated. The parameter and threshold with the highest mutual information was used to split the node into two descendants called child nodes. The samples of the (original) parent node were correspondingly

divided over the two child nodes. Starting with only one node containing all samples, called the root, the tree was constructed by repeating this process until no more splits were possible. No further split was applied to an external node if no additional information could be obtained (Mutual Information was zero), if all the samples reaching this node belonged to the same class (pure class membership), or if the node contained a minimum number of samples, in our case three. By maximizing the mutual information gain at each partitioning step (split), the size of the final decision tree, needed to yield a certain global information, was minimized. After the construction of the tree, the classification took place in the external nodes: the class with the highest number of samples was assigned to all samples reaching the node. In the case of mixed class membership, errors were made for the classification of the samples belonging to other classes, but by assigning the class with the highest probability, the error was minimized:

Suppose the classification problem with two classes a and b, a<>b, and

P	Parent node
L	Left child-node
R	Right child-node
N_e	error made in node N
N_y	number of samples with class y in node N
N_e	$MIN(N_a,N_b)$

THEN $P_a = L_a + R_a$, $P_b = L_b + R_b$

every sample from the parent node P will be put in either the left child node L, or in the right child node R.

IF $L_a < L_b \wedge R_a < R_b$
THEN $L_e = MIN(L_a,L_b) = L_a$, $R_e = MIN(R_a,R_b) = R_a$
$P_a = L_a + R_a < L_b + R_b = P_b \Rightarrow P_e = MIN(P_a,P_b) = P_a = L_a + R_a = L_e + R_e$

if the child-nodes have equal class assignments, these assignments are equal to the allocation in the parent node and the error stays the same.

IF $L_a < L_b \wedge R_a > R_b$
THEN $L_e = MIN(L_a,L_b) = L_a$, $R_e = MIN(R_a,R_b) = R_b$
$P_a = L_a+R_a > L_a+R_b = L_e+R_e$ \
$P_e = MIN(P_a,P_b) > L_e+R_e$
$P_b = L_b+R_b > L_a+R_b = L_e+R_e$ /

if the child-nodes have different class assignments, the error decreases by applying the split.

This proves that, for a two class decision problem, the error will not increase by splitting a node. The extension of this proof for a multiple class decision problem is trivial.

When splitting a node and assigning its own class membership to its children, the classification results stay the same. This is the worst possible case, with increasing classification results for the other cases. During the construction of a decision tree the Re-substitution error rate R(T) can be calculated. The re-substitution error is the misclassification of the training data set. This is the sum of the misclassification errors in the external nodes:

$R(T) = \Sigma R(t) = \Sigma_{Terminal\ nodes} N_e$
with R the error rate, T the Tree, and t a terminal (external) node.

This re-substitution error, however, decreases with every split in the feature space, yielding an optimal retrospective classification with a very large decision tree. In most cases, even 100% accurate retrospective classification can be achieved, by construction of a completely built tree. All external nodes have pure class membership and no further splitting is necessary or possible. This tree, however, lacks the ability to generalise beyond the training data set: every separate sample of the training data is 'remembered'. This is called over-classification of the training data and is a significant disadvantage of the use of decision trees. Therefore, the retrospective classification results are not suitable to evaluate the ability of a tree classifier to assign class membership to new samples. A compromise has to be found between the retrospective classification results and the complexity of the tree, resulting in an optimal prospective classification.

Some tree algorithms use a stop criterion to end the tree construction, avoiding over-classification. These stop criteria usually apply comparison of the internal error rate (Re-substitution error) to a pre-set value. In this way, however, tree construction can stop before all external nodes are split. This can prevent the occurring of good splits, which provide a lot of mutual information. To exploit all possible splits in a decision tree, we used the Iterative Tree Growing and Pruning (ITGP) algorithm described by Gelfand et al. (1991), as base for the complexity control. This method applies pruning of a completely grown tree to control the complexity. The ITGP

algorithm uses two distinct data sets for the construction of a decision tree. The tree is alternately grown with one data set and pruned with the other Next, the role of the two data sets are exchanged. The misclassification in the data set not used for growing, is used to control the complexity of the decision tree. In our application, we noticed a strong dependency between the structure of the tree and the division of the classification samples over the two populations. Therefore, we adapted the algorithm, so it applies the use of two data sets only to the pruning phase (Giesen et al. 1995a) The decisions were made, based on the information of all samples in the training set With this modification, all classification results increased. However, the structure of the decision tree constructed with the adapted algorithm, was equal to the original tree classifier. With the decisions based upon the total training population, a better global segmentation of the feature space was achieved. Using only biopsy samples with unambiguous benign or malignant histology (Giesen et al. 1994), the retrospective classification results were: sensitivity 84.8% and specificity 70.2%. With cross validation (Breiman et al 1984) an assessment of the prospective classification results for this population were calculated: sensitivity 76.6% and specificity 77.8%.

Conclusion

Four out of five co-occurrence parameters selected by Conners and Harlow (1980), combined with the SNR, were suitable for the quantification of the ultrasound image texture. With a binary decision tree applying the mutual information as decision selector, an appropriate classification algorithm for the differentiation between the texture of benign and malignant prostate tissue was made available.

Chapter IV

IMPLEMENTATION OF THE TISSUE DISCRIMINATION ALGORITHMS†

In this chapter a paper is presented which describes the clinical implementation of the texture quantifying parameters and the binary decision trees When this paper was written, all five co-occurrence parameters were used Today, instead of the parameter 'Correlation', the Signal to Noise Ratio (SNR) is used The paper not only presents the use of tissue discrimination for biopsy locations, but also for parts of or even entire prostate images In the discussion section, the possible difference between longitudinal and transverse scanning is given as explanation for not using radical prostatectomy specimens There is a strong correlation between the texture parameters in the transverse and longitudinal images (Giesen et al 1995b) Therefore, transversal scans of prostatectomy specimens were correlated to histo-pathologic examination of prostatectomy specimens (Giesen et al 1995c) With image analysis, a better localisation and assessment of tumour extension were obtained as with standard TRUS

† Published as: Analysis of ultrasonographic prostate images for the detection of prostatic carcinoma, The *A*utomated *U*rologic *D*iagnostic *EX*pert system.
Huynen A.L., Giesen R.J.B., Rosette de la J.J.M.C.H., Aarnink R.G., Debruyne F.M.J., and Wijkstra H.
Ultrasound in Medicine & Biology, Vol. 20:pp 1-10, 1994.

Abstract

This paper describes a study on the automated analysis of ultrasonographic prostate images. With image processing, tissue characterization in the prostate was performed to assess the probability of malignancy. During prostate examinations, images were recorded at the positions where biopsies were taken. The used samples were divided into three groups. Two of them were used for the construction of a classification tree, and the third was used for the evaluation of this classification A sensitivity of 80.6% and specificity of 77.1% were reached retrospectively. In a prospective way, these results were 80.0% and 88.2%, respectively The prospective predictive value for cancer detection was 85.7% The presented prospective value for image analysis was almost twice as high as the values normally found for prostate examination.

Introduction and literature

In the United States, prostate cancer is the second most diagnosed malignancy in men over 50 years old (Lee et al. 1989a; Waterhouse and Resnick, 1989). It is also the most frequent male urological cancer with a growing incidence, depending on age. When it is diagnosed in an early stage, however, prostate carcinoma is curable (Lee et al. 1989a, 1989b, Shinohara et al. 1989). For the diagnosis of prostatism and the detection and staging of prostate cancer, ultrasound is employed by almost every urologist (Hodge et al. 1989b, Lee et al. 1989a; 1989c, Scardino et al. 1989, Waterhouse and Resnick, 1989; Zielke et al 1985) because it is interactive, easy to use, and a relatively cheap medical imaging technique. The quality of TransRectal UltraSound (TRUS) has been improved markedly in the past few years, and an experienced urologist can detect suspicious lesions in the prostate with reasonable accuracy (Schuster et al. 1986; 1987; Shinohara et al. 1989). However, some disadvantages are still attached to the use of TRUS (Bertermann et al. 1989; Chodak et al. 1986, Dahnert et al. 1986; Hendrikx et al. 1990; Lee et al. 1989b; Loch et al. 1990; Scardino et al. 1989; Schuster et al. 1986; Shinohara et al. 1989; Waag et al. 1991; Waterhouse and Resnick, 1989; Zielke et al. 1985). The appearance of cancer lesions in an ultrasound image can vary, depending on the lesion type, location, and transducer. Malignant tumours can appear anechoic, hypoechoic, or even isoechoic, and therefore not all cancers can be detected with TRUS. In early studies with 3.5 MHz transducers cancer was reported to be hyperechoic. According to Shinohara et al. (1989) this could be explained by the advanced stage of the disease that was found in these studies. In this advanced stage of the disease, corpora amylacea could be responsible for the increased echodensity. Lee et al. (1989c) agreed with this explanation but also reported dystrophic calcification in necrotic tumour tissue to be responsible for the hyperechoic echopattern. With the current 7 MHz transducers with a better resolution, malignant lesions can be detected in an earlier stage, in which they appear anechoic, hypoechoic, or isoechoic. Dähnert et al. (1986) reported that

a focal hypoechoic area, corresponding to a tumour, surrounded by a highly echogenic rim, represented a fibrous reaction in some of their cases. This could explain the positive findings of cancer in biopsies from hyperechoic regions alongside a hypoechoic tumour.

Furthermore, not all hypoechoic regions represent malignant tissue. Image artifacts, benign prostatic disease, or even normal biological structures can have similar appearance (Shinohara et al. 1989). The interpretation of an ultrasonographic prostate image highly depends on the experience and expertise of the urologist and his ability to distinguish between artifacts, benign structures, and cancer (Bertermann et al. 1989; Loch et al 1990; Scardino et al. 1989; Shinohara et al. 1989). The urologist can also use additional knowledge, such as Digital Rectal Examination (DRE) and Prostate Specific Antigen (PSA), to aid his interpretation of TRUS images, and the conclusions drawn are not merely based on the information in the images (Lee et al 1989b; Scardino et al 1989; Schuster et al. 1986; 1987, Shinohara et al 1989). In spite of improvements of the ultrasound equipment regarding resolution and grey scale, the interpretation of ultrasound images is still difficult and subjective. Sensitivity rates from 71% to 97% are reported with specificity ranging from 41% to 79% (Chodak et al. 1986; Waterhouse and Resnick, 1989).

Due to the above mentioned limitations, the malignancy of (TRUS) suspicious lesions is never certain, and puncture biopsies have to be taken for histological analysis of the tissue (Ragde et al. 1988). Moreover, a suspicious lesion is not always visible in the image, while there are other reasons (e.g. PSA and/or DRE) to suspect malignancy in the gland. In this case random biopsies have to be taken. Although biopsies are performed as an outpatient method, the procedure carries the risk of bleeding, infection (Lee et al. 1989c) or even urosepsis (Hendrikx et al. 1990). Ultrasound imaging is non invasive and improvement in the diagnostic accuracy of TRUS will permit a reduction in the number of puncture biopsies.

Computer analysis of the images may improve diagnostic accuracy by providing a more reproducible interpretation of ultrasound images of the prostate (Loch et al. 1987; Schuster et al. 1987) and include textural information which the human observer finds more difficult to perceive Some urologists state that malignancy changes spatial characteristics of the grey tones in the image (texture) (Lee et al. 1989b; Scardino et al. 1989). However, most urologists seem to look only at first order statistics (like local mean grey level), possibly in combination with contextual features as size, shape and regularity of the gland (Dahnert et al. 1986; Hendrikx et al. 1990; Hodge et al. 1989b; Lee et al. 1989a; 1989c; Ragde et al. 1988; Shinohara et al. 1989; Waterhouse and Resnick, 1989). It is possible to display second order statistics or other mathematically derived texture features as first order statistics (eg. colours) to improve their detection by the human observer.

Image analysis is applied in many imaging techniques from satellite photography to light microscopy (Haralick et al. 1973; Haralick, 1979; He et al. 1988). In the field of medical imaging and diagnosis of pathologies, some work has been done to investigate the use of image analysis techniques in the examination of liver, female breast, thyroid and prostate tissue (Bertermann et al. 1989; Finette et al. 1983; Loch et al. 1987; 1990; Oosterveld et al. 1993; Schuster et al. 1986; 1987; 1988; Zielke et al. 1985).

The texture in an image can be characterized in a structural, statistical, or spectral manner (Conners and Harlow, 1980; Galloway, 1975; van Gool et al. 1985; Haralick et al. 1973; Haralick, 1979; He et al. 1988; de Souza, 1982; Wang and He, 1990). With the structural method, 'building stones' are defined. The texture is described by the organisation of these elements in the image. With spectral analysis, repeating patterns are recognized and quantified. The statistical methods describe first and second order statistics about grey tone values and transitions in the image. It is believed that the human mind uses some of this information for its interpretation of images and particularly of image texture (van Gool et al. 1985). Several methods have been described for statistical image analysis (Galloway, 1975; Haralick et al. 1973; de Souza, 1982). Conners and Harlow (1980) compared the grey level dependence (co-occurrence), grey level run length, grey level difference, and the (not statistical) power spectral methods and concluded that the use of the co-occurrence matrix yields the best results. This study, however, was done on generated textures and may therefore not be applicable to ultrasound images. In a pilot study (Giesen and Huynen, 1991), the potential of using the co-occurrence matrix for the analysis of ultrasonic prostate images was examined, and the results were so promising that the study reported in this paper was initiated. A system has been developed for automated analysis and interpretation of ultrasonographic prostate images. This **A**utomated **U**rologic **D**iagnostic **EX**pert system (AUDEX) will be used for the classification of prostate tissue and for the detection of carcinoma. The system is based on an ordinary personal computer with additional image processing hardware and is designed to generate colour-coded images displaying the computed probability of malignancy within small tissue regions of the prostate. In this study five features of the co-occurrence matrix describing the ultrasound texture have been used to classify the tissue type in a training data set (with correlative histopathology) and have then been applied prospectively to other lesions of known histology.

Materials and methods

The system was tested with a Kretz Combison 330 ultrasound scanner. With the system, longitudinal images are recorded using a 7.5 MHz transrectal probe. To avoid problems arising from different scanner settings (like Time-Gain-Compensation), a standard setting was determined, which was suitable for almost all images (Near Gain 0, Far Gain 55, Power 14, Transduce/Receive Frequency 7.5 MHz, Burst 2, FrameFilter 2, LineFilter 1, Reject 20, Enhance 2, SampleAlgorithm 5,

DynamicRange C-2). The images were digitized in a resolution of 512 x 512 pixels with 256 grey tones and stored on hard disk. Only the first biopsy on both sides of the prostate was used, because of disturbance of the tissue by the puncture needle and related changes in the ultrasonographic texture. Before the system was able to classify new images, it had to learn the differences between images from benign and malignant tissue. For this reason, images from tissue with known histology had to be recorded. Two consecutive images were stored from every location where a prostate biopsy was taken. The first one was recorded just before the biopsy was taken (see Figure 3a) and used for further analysis. Because the histology could only be determined from excised tissue, the puncture location had to be known exactly. For this purpose the second image was used, which was recorded just before the biopsy needle was retracted from the gland (see Figure 3b). In this ultrasonographic image, the puncture needle was still visible and determined the area for analysis in the first image. Parameters were calculated in this image at three different locations: the proximal, central, and distal parts of the biopsy area. The parameters were calculated from the co-occurrence matrix; a representation of the grey tone transitions in the image (Haralick et al. 1973). In a pilot study (Giesen and Huynen, 1991; Huynen et al. 1991), five parameters, derived from this matrix, were tested for their use in the classification of prostate tissue:

- Uniformity
- Contrast
- Inverse Difference Moment
- Entropy
- Correlation

The matrices that are used in this study are constructed using the grey tones of neighbouring pixels (distance = 1) as well as pixels with an intermediate distance of 2. The grey tone transitions in the horizontal as well as the vertical direction are used in a window of about 3 by 3 mm.

A first order statistic, Signal to Noise Ratio (mean/standard deviation) was also calculated but did not seem to give any additional information for this classification problem

The correlation between the texture parameter values of all biopsies and the histology of the corresponding tissue was determined with the use of binary decision trees (Gelfand et al. 1991; Huynen et al. 1992; Sethi and Sarvarayudu, 1982); a binary decision tree is a hierarchical representation of the decisions made to obtain a classification. In this study the decisions were made by comparing a parameter value to a certain threshold (determined in the learning process, i.e. the construction of the tree). During the classification of one sample, several parameters were used and compared to the corresponding threshold. In this way the combination of the parameters, instead of only one parameter, yielded the prediction for the presence of

malignancy For the implementation of the image processing and decision tree algorithms no specific software packages were used but all algorithms were implemented at our department.

In this stage of the project, we only wanted to distinguish between benign and malignant pathologies (in the rest of this paper referred to as benign and malignant). Therefore, images associated with biopsy samples of other histology were not used.

Construction of the decision tree from the training set used texture parameters only in the location of each biopsy sample. This data was used to classify a larger region of each ultrasound image by placing a small window (3 by 3 mm) over the image, calculating the co-occurrence texture features in this window, and then colour coding that image region depending on the predicted histological classification produced by the decision tree. Next, the window was shifted and this process was continued until the whole region of interest (which could be the complete image) was analyzed

To investigate whether the sample population was a significant reflection of the total population, the learning progression of the system was calculated. First, a small number of samples was used to construct a classification tree. This classification tree was then used to classify a control group (which was kept constant and contained no samples from the training set), to evaluate the categorization The errors in the classification for the training as well as the evaluation set are plotted in a graph Next, the number of samples in the training set was increased and this process continued until all samples were used.

Results

The results presented here were obtained from 51 patients who had one or more puncture biopsies taken during a regular prostate examination Prediction of malignancy by the AUDEX-system was no reason for biopsy, since the system was still in the learning phase. An average of 1.92 useable biopsies was taken per patient which resulted in 98 tissue samples. Reasons for biopsy were abnormal DRE (number of biopsies $n=55$), elevated PSA (≥ 10ng/ml, $n=70$), and/or suspected TRUS ($n=47$). A total number of 239 images was recorded from patients in the age range 50 to 88 years, with an average age of 68.6 years. Only 98 of them could be used, because the histology of the corresponding removed tissue was unambiguously benign (age ranging from 55 to 82, with a mean age of 68.6 years) or malignant (age ranging from 52 to 88 years with a mean of 71.5). 87 Images could not be used because the histology indicated prostatitis ($n=57$, age between 56 and 84 years with an average of 68 years), severe atypia without proof of malignancy ($n=17$), or other ($n=13$) e.g. "not enough tissue to analyze". 54 Images could not be used because there was no correlation between the image used for analysis and the image used for

	Training set		Evaluation set	
(biopsies)	Negative	Positive	Negative	Positive
Benign	27	8	15	2
Malignant	6	25	3	12

Table II *The classification of the biopsies in both the training and the evaluation set The training set (n=66) is used to construct a classification tree This classification is evaluated using samples (n=32) not included in the training set the evaluation set*

the determination of the puncture location or because the puncture location was not visible The used population contained 52 images of benign and 46 of malignant tissue biopsies. The malignant biopsies were almost all moderately differentiated (38) while 2 were well and 6 poorly differentiated

The used samples were divided into three groups the first two were used for the construction of a decision tree, and the third group was used to give a prospective evaluation of the system (Huynen et al 1992) The training set (groups one and two) contained 66 samples (35 benign and 31 malignant) and the evaluation set contained 32 samples (17 and 15, respectively) The results with these groups are presented in Table II, resulting in the values presented in Table III In Table IV the results are presented for all biopsies separated according to the reason for biopsy

The numbers and values, counting patients instead of biopsies, are listed in Table V In this table the patients are classified according to the worst histology found in their biopsies (the histology of the puncture biopsy that was the least differentiated). Patients with positive histology of cancer but carcinoma was not predicted by the AUDEX-system analysis of the local ultrasound image were reported as false negative A false positive was defined as a patient with no carcinoma detected in either biopsy sample but the system predicted malignancy in at least one biopsy site

	Retrospective	Prospective
Sensitivity	80 6	80.0
Specificity	77 1	88 2
Pred. val. pos.	75.8	85.7
Pred val neg.	81 8	83.3

Table III *The results of the classification, presented in Table II, given in percentages*

	Sensitivity	Specificity	Accuracy
DRE -	4/5 (80.0)	33/38 (86 8)	37/43 (86 0)
DRE +	33/41 (80.5)	9/14 (64.3)	42/55 (80.8)
PSA < 10 ng/ml	7/8 (87 5)	17/20 (85 0)	24/28 (85 7)
PSA ≥ 10 ng/ml	30/38 (78.9)	25/32 (78 1)	55/70 (78 6)
TRUS -	7/7 (100)	37/44 (84 1)	44/51 (86 3)
TRUS +	30/39 (76 9)	5/8 (62.5)	35/47 (74.5)

Table IV *The results of the classification of all samples, separated by the different reasons for biopsy*

In Figure 4 the learning curves of the system are plotted These graphs show the percentage of wrongly classified biopsies for a growing number of training samples If the used training and evaluation set have the same distribution, the numbers for the retrospective (training set) and prospective (evaluation set) error rates will have the same values Therefore, the classification curves for the training and evaluation set have to converge, and the point where they reach the same value is the moment that the training set has become a significant reflection of the total population. Using all samples as training set, with all the other settings unchanged, the retrospective results are. sensitivity 86 0%, specificity 87 0%, predictive positive value 86 0%, and predictive negative value 87.0%. Because all samples are used for training, prospective results cannot be given

	Numbers	Value
Sensitivity	21/25	84.0%
Specificity	18/26	69.2%
Predictive value positive	21/29	77.8%
Predictive value negative	18/22	81.8%

Table V *The classification and results considering patients instead of biopsies Patients are classified malignant, according to biopsy with the least differentiated malignancy Patients are classified benign if all their biopsies are benign*

Discussion and Summary

The sensitivity and specificity reached in this research with image analysis are comparable to, or even better than the results presented for regular prostate examinations. The predictive values presented for routine prostate examinations (DRE, PSA, and/or TRUS) are between 29.2% and 42% (Chodak et al. 1986; Lee et al. 1989a; 1989b; Shinohara et al. 1989). For regular investigations our predictive value was 46.9% for biopsies and 49.0% for patients, but for the image analysis it was between 75.8% (retrospective) and 85.7% (prospective) considering biopsies and 77.8% for patients. Looking at the results of the AUDEX system separated for the different reasons for biopsy, it can be seen that the best results are reached in the groups, not suspected to have a malignancy. Of 4 patients with malignancy missed by the system, 3 had only 1 biopsy recorded for this study and only a small area of the prostate image was analyzed, namely the puncture location. When a larger area was analyzed, the system predicted a malignant lesion near the puncture location (prediction 100% malignancy) surrounded by benign tissue in two patients; one lesion of about 9 by 11 mm, and one lesion of 6 by 8 mm. For the other two patients, a diffuse area was found with prediction ranging from 0 to 100% malignancy, with an average of 35%. Of 8 patients falsely predicted positive by the system, 5 had undergone 2 biopsies, and in these 5 cases the other biopsy was predicted negative. Examples of the analysis and colouring of larger parts of an image are shown in Figure 5b (histology benign) and Figure 6b (histology malignant). With this kind of representation of the probability of malignancy in the ultrasonographic prostate image, suspicious areas can be indicated, and therefore possible biopsy locations can be marked.

An important remark has to be made about the correlation between the histology and the image processing parameters. The images of the punctures are analyzed on three positions, and the outcome of this analysis is used in a majority vote to predict the tissue histology. This was done to compensate for extreme outcomes in the parameter calculations. In the histologic analysis of the tissue, however, the smallest amount of cancer is detected while this could be ignored in our analysis.

In our research we only wanted to discriminate between benign and malignant histology, and therefore the images of biopsies with histology prostatitis were not used. These samples can also be regarded as benign pathology, and a decision tree can be constructed with 109 benign tissue samples, consisting of 52 non-inflamed benign (=benign without prostatitis) and 57 prostatitis samples, and 46 malignant samples. With this population the results of the classification are retrospectively: sensitivity 83.9%, specificity 79.5%, and diagnostic accuracy 80.8%. Prospectively these values are respectively 73.3%, 77.8%, and 76.5%.

Some work is reported on tissue classification in the prostate using image analysis techniques. The image analysis methods used by some authors (Bertermann et al.

Figure 3a

Figure 3b

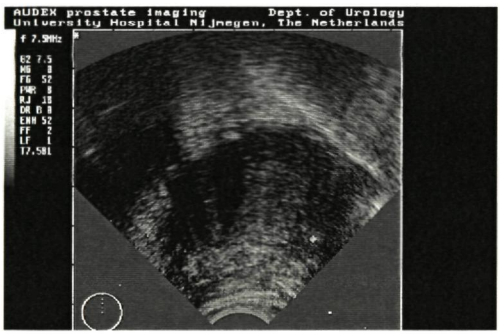

Figure 5a

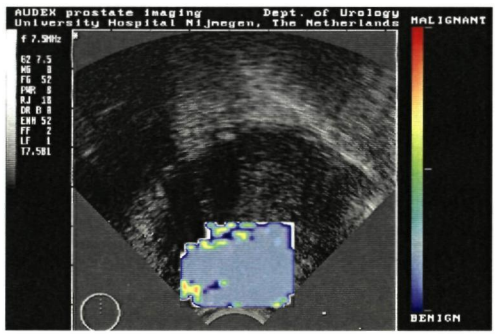

Figure 5b

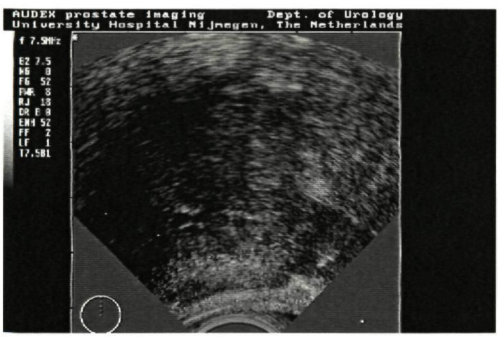

Figure 6a

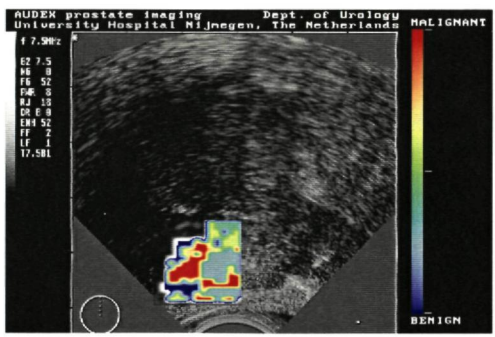

Figure 6b

Figure 3a *The 'clean' image, recorded just before the biopsy is taken In the image the needle is visible (below right) but not yet inserted into the prostate The tissue and corresponding ultrasonographic texture are not disturbed by the needle, and this image is used for image processing and texture analysis*
Figure 3b *The second image, with the biopsy needle still visible in the prostate In this image the puncture location is determined, starting 5mm behind the top of the needle and being 15mm long The removed tissue is analyzed by the pathologist, and the puncture location determines the position for analysis in the clean image (Figure 3a)*

Figure 4 *The learning results of the system Plotted are the percentages of wrong classified samples in the training set and the evaluation set As expected, the curves converge, meaning that the classification might be useful for the interpretation of new images with unknown histology*

Figure 5a *The original ultrasound image of a prostate with benign histology*
Figure 5b *The colour enhanced area displays the computed prediction of the pathology, red symbolizes malignancy, blue indicates benign tissue No malignancy is detected by the AUDEX system or histology of the biopsy sample*

Figure 6a *The original ultrasound image of a prostate found to be malignant on histology The texture appears similar to that in Figure 5a*
Figure 6b *The colour enhanced area predicts malignancy (red) in several regions The prediction of malignancy does not appear to be related to changes in mean grey level but to other textural features not readily perceived in the original ultrasound images*

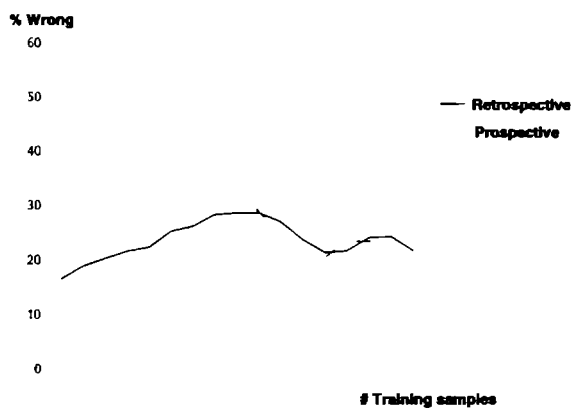

Figure 4

1989, Loch et al. 1987) are not explicitly reported, and it is not clear what influence the image control settings of the ultrasound scanner have Furthermore, the interpretation of objective colour-coded images in their study is still subjective, because some descriptors are coloured and not the probability of malignancy The results cannot be compared because only the sensitivity is given (98 1%). Besides, another difference with our work is that these authors used a specifically developed ultra-fast computer (image analysis system), which may limit the widespread use of the system in a clinical environment Zielke et al. (1985) reported image processing in the prostate and a classification rate of 90%. The settings and conditions of that research, however, are not clearly reported.

Thijssen et al. (1993) investigated the correlation between co-occurrence parameters and acoustic parameters and concluded that the co-occurrence parameters correlated for more than 90%. Because these parameters also correlated to the acoustic parameters, they were not used in their discriminant analysis (Oosterveld et al. 1993). In our case only the uniformity correlated strongly with the other parameters When this parameter was omitted from the tree construction, the retrospective results were sensitivity 73.5%, specificity 69 4%, predictive value positive 69 4% and predictive value negative 73.5 %. For the prospective results these values were· sens 68 8%, spec. 84.2%, pred pos 78 6% and pred.neg 76.2% The parameters used in this classification were contrast, inverse difference moment, and entropy.

Ultrasonographic tissue discrimination has some disadvantages the lack of homogeneity of the tissue, place dependency (distance to the echoprobe) of texture in ultrasonography, and dependence on scanner settings (Morris, 1988; Schuster et al 1987, Zielke et al 1985) With our approach the system can easily be coupled to any ultrasound machine. However, we did not investigate the influence of the characteristics of different scanners, transducers, and control settings Because these may influence the image processing parameters, a training data set has to be recorded for every scanner/transducer/control-setting. If the influence of these characteristics can be measured and separated from the influence of the tissue structure, only one decision tree will be necessary for all scanner/transducer/setting-combinations.

From the graphs of the learning curves, it can be concluded that the used training set reaches the same distribution as the evaluation set. This means that the classification of this population might be used to assess tissue histology in ultrasonographic prostate images. The used population, however, is not a significant sample for analysis of the whole prostate. All images are taken from biopsies, and hence the locations for analysis are mostly situated in the peripheral zone. Consequently, if the system has to be used to predict histology in other zones of the prostate (e.g. transition zone), the training set has to be extended with samples from these zones. One way for doing this is the use of radical prostatectomies; images of

the whole gland can be recorded and after analysis compared to the histology of corresponding slices of the prostate (Dahnert et al. 1986; Hendrikx et al. 1990, Shinohara et al. 1989) In this way the samples are uniformly distributed over the whole prostate. Another way to obtain material from other parts of the gland is the use of tissue removed by TransUrethral Resection of the Prostate (TURP). About 10% of the patients who are surgically treated (TURP) for benign prostatic hypertrophy have a malignant disease of the prostate (incidental prostate carcinoma), which is usually not TRUS suspicious (Waterhouse and Resnick, 1989). In our study no radical prostatectomies are used because the histological sections are made transversally, while the images that we use for our training set are longitudinal (puncture-) images. No TURP-material was used because there is no clear correlation between the image and the removed tissue (Hendrikx et al. 1990), since only the side of the gland where the tissue was removed is known.

In this stage of the project only standard image interpretation parameters were used No specific parameters for the analysis of ultrasonographic (prostate-) images or the detection of cancer were used In the future, clinical information about prostate cancer, like DRE or PSA, will be imbedded in an artificial intelligence system, and combined with decision trees to produce the colour coded images of probability of malignancy In this way it will also be possible to investigate the relative importance of the clinical data. The disadvantage of a parameter like PSA, however, is that it is not correlated to specific positions in the image and therefore cannot indicate the puncture location, while image processing parameters can do this very precisely.

The results presented in this paper are obtained with a decision tree constructed with equal weights assigned to errors in malignant and benign predictions. This means that a wrong malignant prediction (false positive) causes the same error rate in the classification tree as a benign misclassification. By adjusting these weights, one of the predictive values (positive or negative) can be emphasized, according to the needs for a specific study or examination (e.g. screening).

The AUDEX system has the potential of playing an important role in routine clinical practice It has the advantages of being able to quantify texture features, some of which can not be observed by the urologist. An estimation of the probability for malignancy, derived from the correlative textural and histological data in a training set, can be presented in image format and compared to the original ultrasound B-scan image. This provides additional information especially in images with no visible lesion, which may assist the urologist in judging whether or not and where to take a biopsy.

These results have encouraged us to commence a multi-centre clinical trial in three Dutch hospitals (Nijmegen, Eindhoven, and Breda). For all the three hospitals a training dataset is recorded and a corresponding decision tree is constructed. In this study the results of the AUDEX system will be used to direct additional biopsy sites

not located using normal diagnostic methods (DRE, PSA, and/or TRUS) and further examine the accuracy of the AUDEX system for predicting malignancy.

Acknowledgement

The authors would like to thank Prof. J.M. Thijssen, Ph.D., M.Sc. for his helpful criticism in the preparation of this manuscript.

Chapter V

IMPACT OF AUTOMATED IMAGE INTERPRETATION ON CLINICAL DECISION MAKING

Abstract

This chapter describes a prospective comparison of standard diagnostic methods for the detection of prostate carcinoma to automated detection utilising computer analysis of TransRectal UltraSound (TRUS) images of the prostate. As clinical diagnostic tools, Digital Rectal Examination (DRE), serum Prostate Specific Antigen (PSA) level, and human interpretation of TRUS images are used. For the automated analysis, the correlation between quantified textural information and the histology of tissue biopsies is used. For a prospective evaluation, the classification results of the clinical diagnosis as well as the automated image interpretation in the patient population with prostatism complaints are calculated. For this calculation, a biopsy rate of 10 % is assumed, while the frequency of incidental carcinoma is taken from literature as well as from biopsies in patients without clinical suspicion for prostate carcinoma. Using these values, the True Negative and False Negative rates for the clinical diagnosis are calculated. In the population with prostatism complaints, the sensitivity for cancer detection of automated analysis is 2.6 times higher than for the normal clinical diagnosis. The classification accuracy of this population is 2.5 times better (using the Receiver Operating Characteristic) for the automated categorisation. Prospectively, automated image interpretation has a much higher tissue discrimination performance than standard clinical methods in the patient population with prostatism complaints.

Introduction

Medical ultrasound images are produced by transmitting ultrasound waves through the organ to be visualized. The reflected sound waves are recorded and represented as grey values on the screen of the ultrasound scanner (Russell and Resnick, 1979; Wells, 1977). Pathology changes the tissue reflecting the ultrasound waves and might, therefore, influence the reflection properties of this tissue. In this way, pathologic tissue can differ in appearance on ultrasound images from benign tissue. This thesis demonstrates that the differences in ultrasonographic texture caused by pathology can be used by a computerized system to differentiate between the different histology types. Because the pathologic changes in the tissue are reflected in the textural features and these pathologic changes will be the same for clinically normal (negative diagnosis) as well as cancer-suspected (positive diagnosis) prostate tissue, the correlation between textural features and tissue histology in a select population with puncture biopsies performed will be equal as for the total population with prostatism complaints.

Until now, however, the classification results were only calculated for the patient population with clinical suspicion for prostate cancer. This is a strongly selected population, not comparable to the total patient population with prostatism complaints. Because this selection is made by the clinical diagnosis, no evaluation of this

diagnosis can be made in this population. Furthermore, the histology of the patients not biopsied is unknown. This has the disadvantage that no prospective comparison can be made between the standard clinical diagnostic tools and the automated image interpretation. A combination of the separate clinical diagnostic factors is used to yield the overall clinical diagnosis. The clinical diagnosis is defined as suspicious for carcinoma if at least one of the clinical diagnostic factors (DRE, TRUS, or PSA-level) showed suspicion. From the histology of the tissue samples, removed with puncture biopsies, the rates of True Positive (TP) and False Positive (FP) are calculated The histology of the patients with no suspicion for prostate cancer is unknown and the rates for True Negative (TN) and False Negative (FN) can not be calculated. Therefore, no values for sensitivity, specificity or predictive value of the negative test outcome can be calculated for the total population. For the population undergoing puncture biopsies, these values can only be calculated if another definition of positive and negative test outcome is used (because, with clinical diagnosis, all samples in this group are classified positive). This can be done by looking at the separate diagnostic factors (DRE, PSA, or TRUS) one at a time. Furthermore, for the PSA value, different cut-off values can be taken For example, a cut-off value of 4 mg/l is used as threshold to perform biopsies A threshold of 10 mg/l can be used to split the selected puncture population into a positive and negative 'tested' sub-population.

To assess the classification results in the total population, estimations have to be made about the prevalence of malignancy in the part of the population without clinical suspicion of malignancy This estimation can be based on the rate of incidental carcinoma found after TransUrethral Resection of the Prostate (TURP). Another method is to perform puncture biopsies in patients, independent of the probability of malignancy. In a small group of patients visiting the out-patient clinic, puncture biopsies were performed to examine the treatment outcome of TransUrethral Microwave Thermotherapy (TUMT) on the different benign histology types and to exclude carcinoma for non-surgical therapy for Benign Prostatic Hyperplasia, like TUMT, TransUrethral Laser Induced Prostatectomy (TULIP), or Visual Laser Ablation of the Prostate (VLAP). The biopsies taken from these patients with clinical benign diagnosis give us the opportunity to investigate the cancer prevalence in the non-suspected patient population.

For the automated tissue discrimination the same problem arises. no actual classification results can be calculated for the non-suspected population. The textural features, however, are calculated from tissue with normal as well as abnormal ultrasound images and are independent of the ultrasound suspicion of the tissue. Furthermore, it seems plausible that these features are independent of the other clinical parameters (DRE and PSA). Therefore, the textural features of benign and malignant tissue are not correlated to the clinical diagnosis of this tissue. Assuming the textural image properties to be the same for the selected population as for the total population, sensitivity and specificity for cancer detection using the computer system are expected to be the same in a non-selected population. Furthermore, only

minor differences exist for the automated classification if the samples are separated by the different diagnostic tools and the automated classification yields better results for negative test outcomes in the clinical diagnosis (Huynen et al. 1994) With fixed decisions, sensitivity and specificity values are not dependant on the prevalence of disease (Zweig and Campbell, 1993), because they are calculated from the malignant respectively benign samples only. Consequently, the sensitivity and specificity of the decision tree calculated from the puncture biopsies, can also be used for the total patient population. For this calculation the prospective classification results of the decision tree must be used. Using cross-validation, the classification of each sample can be predicted without incorporating it into the training process of the decision tree. With the prospective values for sensitivity and specificity and the rate of malignancy in the patient population, the predictive values of positive and negative test outcomes can be calculated. The rate of malignancy is the same as calculated for the clinical diagnosis, because it is calculated for the same population.

Material and Methods

From 282 biopsies, all clinical diagnostic parameters and the tissue histology are known. For these biopsies, the clinical suspicion (using a cut-off value of 10 mg/l for the PSA level) yielded the following classification results True Positive (TP) n = 79, False Positive (FP) n = 150, True Negative (TN) n = 51, and False Negative (FN) n = 2. For the different diagnostic predictors, the classification was compared to the automated interpretation of the ultrasound images. Also the combination of the diagnostic tools as clinical diagnosis was evaluated.

Using the diagnosis made during the clinical investigation, all biopsies had a positive test outcome. The values of TP and FP were 81 and 201. These numbers

	TRUS	DRE	PSA ≥ 10ng/ml	Clinical suspicion	Computer analysis
Sensitivity	73.7	84.2	69.5	97.5	76.6
Specificity	84.4	77.8	43.1	25.4	77.5
Pred.Val.Pos.	66.7	61.5	34.0	34.5	59 0
Pred.Val.Neg.	88.4	92.1	77.0	96.2	88.7
ROC-distance	41.1	43.8	8.9	16.0	38.3

Table VI *The classification results for cancer detection, obtained in a select population with suspicion of prostate cancer*

were used for the population with positive clinical test outcome (suspicion for prostate cancer). Biopsies were performed in 10% of the patients visiting the outpatient clinic. This means that a total of 100/10*282=2820 biopsies would have been performed if all patients visiting the outpatient clinic would have had puncture biopsies. From the 'non-performed biopsies' (n = 2820-282 = 2538), the tissue histology was estimated using the value of incidental carcinoma found in the biopsies performed of the clinical negative patient group. Malignancy was found in 5 out of 65 patients undergoing biopsies without clinical suspicion of prostate cancer. This means that incidental carcinoma was found in 7.7% of these patients. This number was used, together with the numbers of incidental carcinoma presented in existing literature for TransUrethral Resection of the Prostate (TURP), as assessment of the malignancy rate in the clinically benign group. Values in literature range from 10% to 20% (Bostwick et al. 1992, Lowe and Listrom, 1988; Mebust et al. 1989; Peeling and Griffiths, 1984) Caused by the high predictive value for negative test outcome, necessarry to exclude carcinoma for non-invasive therapy for BPH, the rate of incidental carcinoma found at TURP in our clinic was only 5% Using all these percentages for incidental carcinoma, the values for TN and FN were calculated. Together with the values of TP and FP, prospective classification results for the clinical diagnosis as well as the automated interpretation of the ultrasound images were calculated The conclusions of this chapter will be based on the ratio incidental carcinoma of 7.7%, as found in the biopsies of patients with clinical benign diagnosis.

	Incidental Carcinoma				
	20%	15%	10%	7 7%	5%
Sensitivity	13 8	17.5	24.2	29.3	39.0
Specificity	91.0	91.5	91 9	92.1	92.3
Pred Val.Pos Clin.Diagnosis	28 7	28 7	28 7	28.7	28.7
Automated	47.3	40.0	31.4	27.0	21.3
Pred Val.Neg.Clin.Diagnosis	80.0	85.0	90.0	92.3	95.0
Automated	92.6	94.4	96.1	96.8	97.7
ROC-distance	3.4	6.4	11.4	15.1	22.1
Gain	34.9	31.9	26.9	23 1	16.1
Improvement	11.4 x	6.0 x	3.4 x	2.5 x	1 7 x

Table VII *Prospective classification using a value of 4 mg/l for the PSA level as threshold to suspect malignancy*

Results

Table VI presents the retrospective classification results for the different diagnostic tools and their combination and the automated image interpretation. These are the classification results in the population with clinical suspicion for prostate cancer. In this table a cut-off value of 10 mg/l was used in the PSA-level as threshold for suspicion of malignancy. For the clinical diagnosis, these values are retrospective results because the patient population was selected using the same criteria (except for a different PSA-threshold). The automated classification results are prospective values for the same population, calculated using cross-validation. The ROC-distance is a combination of the sensitivity and specificity and yields an overall quantification of the classification (Giesen et al. 1994).

Table VII presents the prospective classification results for the total patient population with prostatism complaints For the calculations in this table, a threshold of 4 mg/l was used for the PSA level, because this is the value used during clinical investigations. We see that the sensitivity for the total population with prostatism complaints is much lower than in the selected sub-population with suspected prostate cancer. The sensitivity and specificity of the automated method in this population were equal to the prospective values presented in Table VI. The presented ROC-distance was calculated for the clinical diagnosis. The automated method had a constant ROC-distance of 38.3. The gain is the difference between the ROC-distance of the automated method and the diagnosis and the improvement is the ratio of these two values.

Using the ROC-distance to evaluate the classification results, the automated method improved the tissue discrimination by 150%, using 7.7 % as rate of prostate cancer in the clinically non-suspected group as detected with puncture biopsies.

Discussion

Table VI shows that for the select population with clinical suspicion of prostate cancer, the automated image interpretation is slightly less accurate than a single TRUS or a single DRE. Due to a high number of false positives selected by PSA, the overall clinical diagnosis is not as good as single DRE or single TRUS. Although the sensitivity for the automated method is not as high as for the clinical suspicion, the specificity for the automated method compensates the overall classification results. This population is selected by a clinical suspicion for prostate cancer. Because this selection is based on the different clinical investigation tools, the sensitivity for the clinical suspicion is very high. The sensitivity for the separate diagnostic factors will be biased, because the DRE was performed with knowledge of PSA levels and TRUS was performed with knowledge of DRE and PSA levels.

The values used as indication of incidental carcinoma in Table VII are estimations. Only a small number of patients with clinical benign diagnosis has had puncture biopsies. Furthermore, when carcinoma is not found with biopsies, it is not absolutely sure that there is no carcinoma present. The percentage of incidental carcinoma can, therefore, be higher as well as lower than used for the calculations. Furthermore, the calculations are done for the population of patients with prostatism complaints The prevalence of prostate cancer, as well as the clinical diagnosis for the total male population, is unknown. However, even with a percentage of incidental carcinoma of only 2% for the patients with prostatism complaints, automated image interpretation provides better tissue discrimination than ordinary clinical diagnostic tools.

For the clinical diagnosis, as well as the automated image interpretation, no actual prospective classification results can be calculated for the population at risk At this moment, however, no consensus is reached whether early detection of (all) prostate carcinoma is desirable, because the influence of early treatment on mortality and morbidity are unknown. The American Cancer Society (-National Prostate Cancer Detection Project) is currently investigating the impact of DRE, PSA, and TRUS for early prostate cancer detection on cancer mortality (Mettlin, 1993). Unfortunately, results of this study will not be available until the year 2010, due to the long follow-up required.

In existing literature, the presented values for cancer detection with TRUS range from 68% to 92% for sensitivity and from 41% to 79% for specificity (Chodak et al. 1986; Scardino et al. 1989; Waterhouse and Resnick, 1989) Compared to these values, our study found a small preference for benign prediction with TRUS (the specificity is higher). In contrast to results in existing literature, DRE showed a higher sensitivity for cancer detection than TRUS, but the accuracy was better for ultrasound. The high inter-study variability for TRUS, supposes a high subjectivity resulting in a low reproducibility for human interpretation of ultrasonographic images. Bertermann et al. (1989) reported the use of computer assisted analysis of ultrasound images for detection of malignancy in the prostate Zielke et al. (1985) stated that computer analysis of prostate images increases the accuracy and reproducibility of interpretation of ultrasound images and that it reduces the need for intensive investigations. These reports, however, only quantified the textural features in the ultrasonographic images without automated correlation to the tissue histology. Furthermore, no results are presented for all classification values so no comparison is possible for our automated method.

For the classification of the computerized system, no distinction is made between False Positive and False Negative misclassification rates. Therefore, the values for sensitivity and specificity are in the same range. Additionally, automated analysis of the ultrasound images uses only local image properties. For different study designs, the weight factors for the different histology types can be adjusted and the sensitivity and specificity will be modified accordingly. Furthermore, the automated interpretation

can be used as an addition to the standard clinical diagnostic tools, combining the advantages of all methods.

Conclusion

This chapter shows that the sensitivity for cancer detection in a population selected with standard diagnostic methods is higher with these standard diagnostic methods than with a computerized system The classification results of the automated system in the select population with suspicion for prostate carcinoma were comparable to single DRE and especially to single TRUS. However, automated classification does not depend on human interpretation and is, therefore, less subjective, more accurate, and more reproducible. Compared to the combination of clinical diagnostic factors, the automated method had a much lower sensitivity in this population due to the biased sensitivity for the clinical diagnosis. The total classification is better for the automated method, because of a large increase in specificity.

For the population with prostatism complaints, the standard clinical diagnostic tools only recognized 29.3 percent of the prostate cancers. With the automated method, 178% more biopsies would have been taken (n = 784) as with the standard clinical methods (n = 282) This higher number of biopsies, however, would also increase the sensitivity from 29.3% to 76.6% and the ROC-distance (overall classification) from 15.1 to 38.3 The predictive value of a positive test outcome was slightly less, while an increase was seen for negative test outcomes.

We conclude that a computerized system can be very helpful to the urologist in the interpretation of the ultrasonic prostate images. Using these techniques, the interpretation of ultrasound images will be improved and the detection rate for carcinoma in the prostate will be increased. Furthermore, a computerized system can be a very useful primary tool in prostate cancer screening programs, performed on the out-patient population, because of its high predictive value for the negative test outcome (96 8% versus 92.3% for the clinical diagnosis, assuming 7.7% carcinoma in the clinical negative group). Only patients with a positive prediction for prostate cancer by the automated method need to be tested by a urologist.

Chapter VI

MULTIPLE HISTOLOGY-CLASS TISSUE DISCRIMINATION

Abstract

The automated tissue discrimination algorithms were extended to be able to discriminate more histology types. Incorporating the biopsy samples with inflamed histology (prostatitis), the discrimination between benign and non-benign histology (prostatitis combined with malignant samples) was tested, as well as the differentiation between malignant and non-malignant histology (prostatitis combined with benign histology). Also the classification of the three histology types separately was evaluated. The ultrasonographic texture of the inflamed and benign prostate tissue were simmilar, reflecting comparable histologic appearances. Therefore, the automated method was not capable to discriminate between the three histology types. The sensitivity for carcinoma detection will increase by the extension of the benign biopsy group with the samples of inflamed prostate tissue.

Introduction

The methods described in this thesis for the determination of tissue histology were developed for the detection of prostate carcinoma. For this purpose, only the distinction between benign and malignant histology was used and only biopsies with unambiguous benign or malignant histology were included in the training data set. Compared to other histology types, it is unknown whether the automated tissue discrimination algorithms detect malignant or benign tissue. However, during clinical investigations, not only tissue with benign or malignant histology is examined, but also inflamed prostate tissue. For small biopsy populations, two studies were performed incorporating biopsies with the histology prostatitis (inflamed prostate tissue). In Chapter IV, the prostatitis samples were used together with the benign samples to form the group of non-malignant biopsy specimens. Also the discriminating power was evaluated between the image texture of the benign histologies and prostatitis without using the malignant samples (de la Rosette et al. 1995). The classification results of these two investigations raised the question whether the automated classification process can be used for a multiple histology class tissue discrimination process for the classification of benign, malignant, and inflamed tissue simultaneous. For this investigation, the implementation of the decision tree algorithm was extended to be able to classify multiple histology class tissue samples. Also the detection of benign versus non-benign histology and of malignant versus non-malignant histology was tested.

To be able to represent three histology types, the presentation of the predicted tissue types as colour-coded projections into the ultrasound images has to be extended. The colour coding in the two-class discrimination processes used a temperature scale to represent the different histology types. The probability of malignancy is coded to a position on this scale and the corresponding colour is projected into the original ultrasound image. This method is not applicable for a

multiple tissue type classification problem because the probabilities for three or more tissue types (including benign tissue) have to be represented with one colour. A solution can be the construction and presentation of one colour coded image for each histology type In this image, only the probability of one particular tissue histology is presented, possibly after applying a threshold to restrict the colour coding to the image regions representing the tissue type with maximum likelihood. A disadvantage of this method is the presentation and, therefore, the need to interpret multiple images simultaneously Also the compression of the images, needed to fit them on one monitor, reduces the information extraction capacity For the classification of benign, malignant, and prostatitis tissue (or any other combination of three histology types), the similarity between the use of three tissue type classes and the composition of coloured images from three components yields a possible solution to this presentation problem. The Red, Green, and Blue components of the (RGB-coded) colour for the projection of the predicted tissue histology can be based on the probabilities of the three different histology types. A triangle is constructed with each corner corresponding to 100% probability of one tissue type. The side opposite to each point represents 0% probability of this kind of tissue. In this way, all combinations of tissue histology types (the summation of these probabilities is 100%) can be represented by exactly one position in the triangle. By colouring the triangle according to the three components of the colour scale (Red, Green, and Blue), every position in the triangle, i.e. every combination of predicted histology classes, corresponds to exactly one colour. For psychological reasons, it is best to represent a potential hazardous tissue type (in this case malignancy) with red and a harmless histology (benign tissue) with blue. This leaves green as the representation of inflamed prostate tissue (prostatitis).

Material

The total biopsy population consisted of 229 biopsies with benign histology, 102 biopsies with malignant histology, and 80 biopsies with inflamed tissue (prostatitis). The prostatitis biopsies were first combined with the biopsies with benign tissue to yield a group of non-malignant tissue samples. This combination was used to examine the carcinoma detection rate in a population, similar to the patient population investigated by the urologist. Also the combination between prostatitis samples with malignant samples was tested against the benign biopsies to evaluate the detection rate of tissue abnormalities (deviations from benign tissue). The evaluation of prostatitis against non-prostatitis tissue seems to have no clinical value because it implies the combination of benign and malignant tissue. Therefore, this third combination of the three histology classes as a two-histology class decision problem was omitted. After the two-class decision problem investigations, every histology was used as a separate decision class, yielding the classification problem Benign-Malignant-Prostatitis. For every classification problem the optimal tree setting was determined using cross-validation and the prospective ROC-distance. Using this

	Histology		
	Benign	Malignant	Total
Benign	169	31	200
Malignant	60	70	130
Unknown	0	1	1
Total	229	102	331
Correct	73.8 %	68.6 %	30.0†

Table VIII *Automated classification of biopsy samples with benign and malignant histology*
† *ROC-distance*

setting, the prospective classification results were calculated.

With a two-class decision problem, the ROC distance is a combination of the sensitivity and specificity of one of the classes. Because the sensitivity of one class equals the specificity of the other class, it can also be seen as a combination of the sensitivities (or specificities) of the two classes. With three classes, however, the sensitivity of one class is not directly related to the specificity of the other classes. The ROC-distance for the overall classification of three classes can not be calculated directly from the sensitivities or the specificities of these classes. Therefore, a combination of the sensitivities and a combination of the specificities are both used for the calculations. For the evaluation of the sensitivities, the distance to the plane

	Histology		
	Benign	Non-Benign	Total
Benign	140	68	208
Non-Benign	88	113	201
Unknown	1	1	2
Total	229	182	411
Correct	61.1 %	62.1 %	16.4†

Table IX *Automated classification of biopsy samples with benign and non-benign (i e malignant or prostatitis) histology*
† *ROC-distance*

$Sens_1 + Sens_2 + Sens_3 = 100\%$ is calculated, while the specificity is related to the plane $Spec_1 + Spec_2 + Spec_3 = 200\%$. Both planes represent a classification with no information gain compared to gambling with a priori knowledge; this corresponds to the line Sensitivity + Specificity = 100% in the two class problem.

Every biopsy was analyzed at three image locations (proximal, central, and distal) and the three class assignments, corresponding to these locations, were used in a majority vote to label the biopsy. A disadvantage when using more than two histology type classes is a possible lack of a majority vote for the classification of all three image-samples belonging to the same biopsy. This majority vote was used to correct for small misclassification errors; if only one image-sample of a biopsy was misclassified, the majority vote selected the correct classification for the entire biopsy area. With more histology types present, it could occur that all samples from the same biopsy had a different histology assigned by the automated method. If this was the case, the biopsy was classified as 'unknown'.

Results

Table VIII presents the classification of benign and malignant samples. Table IX shows the prostatitis samples classified together with the malignant samples, representing the group with deviations from benign in the tissue histology. Table X presents the classification of the two-histology class decision problem malignant versus non-malignant. In the tables, the correct classification rate for a class (in the tables presented as 'correct') equals the sensitivity for that class These tables show

	Histology		
	Non-Malignant	Malignant	Total
Non-Malignant	195	23	217
Malignant	114	78	193
Unknown	0	1	1
Total	309	102	411
Correct	63.1 %	76.5 %	28.0†

Table X *Automated classification of biopsy samples with malignant and non-malignant (benign or prostatitis) histology*
† *ROC-distance*

that addition of the prostatitis samples to the benign biopsy group does not have a large influence on the overall classification results, while combination of the malignant and inflamed tissue samples yields a strong decrease in classification. Although the overall classification of malignant versus non-malignant samples is comparable to the benign versus malignant classification, an increase in sensitivity for the malignant group can be seen, at the cost of the specificity (equals the sensitivity of the non-malignant group).

In the two-class decision problems, samples are classified as unknown although a majority vote over three analysis regions, together with two histology classes, should not be a problem. During the analysis of an image sample, however, the grey tone transitions in the analysis region are tested and if more than 15% of these transitions include a grey value of zero, not enough information is present and that area is not analyzed. If one of the three analysis regions of a biopsy is not analyzed and the other two have different class assignments, no majority vote can be applied

Table XI shows the classification results for the three-histology class discrimination problem. Using the ROC-distance for the evaluation, the overall sensitivity of this classification is slightly less than for the discrimination between benign and malignant, or between non-malignant and malignant tissue. Especially the sensitivity for the prostatitis tissue is very low. However, the specificity is high for the prostatitis samples, while the overall specificity for this three class problem is disappointing. A small number of biopsies (n = 14, 3.4 %) could not be classified because each analyzed image sample had a unique histology assignment The percentage of un-classified samples was the highest for the prostatitis samples and lowest for the malignant specimens.

	Histology			
	Benign	Malignant	Prostatitis	Total
Benign	145	16	39	183
Malignant	48	59	17	140
Prostatitis	27	24	20	74
Unknown	9	3	4	14
Total	229	102	80	411
Sensitivity	63 3 %	57.8 %	25.0 %	26.6†
Specificity	65.9 %	74 8 %	81.0 %	12.5†

Table XI *Automated classification of biopsy samples with benign, malignant, or prostatitis histology*
† *ROC-distance*

Because the classification results with three histology classes are discouraging, it is pointless to colour-code ultrasonographic images according to this classification. Therefore, the presentation of three histology classes in an ultrasound image is omitted.

Discussion

The overall classification of malignant samples versus non-malignant samples is comparable to the classification of malignant versus benign tissue This can be caused by the ultrasonographic appearance of malignancy, different from benign and prostatitis tissue, together with a similar appearance of the latter two. After reviewing the histopathology of the biopsy samples, we found reasonable overlap between the benign and prostatitis histologies (Giesen et al. 1994). This reveals the pathologic similarity between the two tissue types, possibly reflected in the ultrasonographic appearance. This assumption is strengthened by the classification of the three histology classes, in which the majority of misclassified prostatitis samples was categorized as benign. Another explanation can be the optimization of the tissue discrimination algorithms for the determination of malignancy. An improved discrimination of three histology classes may be achieved with other, or additional texture quantifying parameters, or with an optimization performed for the three histology classes. The classification of benign versus prostatitis tissue samples, as presented in an earlier paper, contradicts these hypotheses (de la Rosette et al. 1995). With an increased biopsy population, however, the detection rate of prostatitis tissue strongly decreased, indicating a large overlap between the texture quantification of benign and inflamed tissue.

For detection of carcinoma using the automated tissue discrimination algorithms during clinical investigations, i.e. with the addition of prostatitis samples to the benign group, an increase in biopsy rate from 39.3 % to 47.0 % can be seen, accompanied by a decrease in predictive value

In this investigation, the addition of prostatitis samples was examined to yield a classification problem, resembling the clinical investigative situation. However, the three histology types benign, malignant, and prostatitis are not the only tissue types present in the prostate. Other tissue types like Necrosis or Prostatic Intraepithelial Neoplasia, can also be found in the gland. Influence on the classification process, however, is unlikely, due to the small occurrence (6.6 %) of these histology types.

Conclusion

The addition of prostatitis samples to the benign population has only minor influence on the overall classification results. The classification of three histology

classes, or the detection of abnormalities in the tissue (deviation from benign, i.e. malignancy or prostatitis) is inaccurate, with the parameters and settings as derived for the detection of prostate carcinoma. With these classification results, it is needless to implement a colour-coding algorithm for the presentation of three histology classes. The results during clinical examinations will not be affected negatively by incorporating the prostatitis samples, caused by similar pathologic as well as ultrasonographic textural appearance of prostatitis and benign prostate tissue. The specificity for carcinoma detection will decrease, accompanied by an increase in sensitivity. This is caused by the increased relative homogeneity of the group of malignant samples in the training set.

Chapter VII

POSITION DEPENDANT ENHANCEMENT OF ULTRASONOGRAPHIC TEXTURAL FEATURES†

† A.L. Huynen, R.J.B. Giesen, R.G. Aarnink, J.J.M.C.H. de la Rosette, F.M.J. Debruyne, and H. Wijkstra. *Submitted, Ultrasound in Medicine & Biology, 1995*

Abstract

This chapter describes position dependencies of statistical image processing parameters in ultrasonographic images. The dependency is investigated on the angle of the scan line in the image for a single element transducer and a pre-processing step is introduced to reduce this dependency. The depth dependency for this transducer is also examined. Pre-processing algorithms turned out to be insufficient for the correction of the depth dependency. Therefore, regression curves are calculated for images of tissue mimicking phantom material, to compensate the depth dependency afterwards. The correction algorithms are evaluated for the tissue discrimination of the biopsy samples. The classification of ultrasound images of the biopsies is performed with and without the described corrections. With only one of the corrections performed, the classification results decrease. With both corrections performed, the overall classification improves. The specificity reaches a higher value, but the sensitivity slightly decreases.

Introduction

The method for tissue discrimination has one drawback: the physics of ultrasound produce in-homogeneous images (Hill et al. 1991; Oosterveld et al. 1985; Wells, 1977). A number of phenomena in ultrasound imaging contribute to dependencies of the imaged reflection properties on the distance to the ultrasound transducer: the shape (and focus) of the ultrasound beam, interference patterns of the reflected sound waves, attenuation, and corresponding Time Gain Compensation. Because of these circumstances, the speckle pattern varies in the image, depending on the distance to the ultrasound transducer. This depth dependency may be reflected in the texture quantification of the images. Furthermore, because a single-element transducer is used, the scan lines are not parallel but rotating in the image (polar coordinates). Therefore, the direction in which the speckle pattern is oriented is dependant on the angle of the scan line. The image, however, is constructed in an orthogonal grid produced by the quantification of the video signal. The co-occurrence matrix is constructed in the orthogonal grid, originated from the use of the video signal, and, therefore, an angle dependency will be expected for the co-occurrence parameters in the images. Besides the depth dependency caused by the physics of the ultrasound beam, further depth dependencies are introduced. The scan lines for a single-element transducer spread with the distance to the ultrasound probe and the resolution decreases with increasing distance. Less information is retrieved in lateral direction from the reflected ultrasound signal and the grey value of a larger number of pixels will be determined by interpolation of the grey values of the neighbouring pixels.

For the tissue discrimination algorithms, the calculated correlation between the parameter values and the tissue histology is determined at the biopsy location in

recorded puncture images. This location is at a variable position along a fixed line in the images and the training population may not be a significant spot check of the tissue visible in the total image. To use the calculated correlation as an applicable analysis for total images, a position dependent correction for the parameter values has to be determined. The corrected parameter values of a homogenous tissue type will have to yield the same values, independent of the position in the ultrasound image where this tissue is visualised. Because the depth and angle dependencies are independent phenomena, both position related deviations and the associated corrections were investigated separately.

In this chapter the angle and depth dependencies are investigated in images of tissue mimicking phantom material. According to the dependencies in this material, correction algorithms are developed. These correction algorithms are used for the automated interpretation of ultrasonographic prostate images and evaluated for the classification of tissue histology of biopsy specimens. The classification results of the biopsies will be tested with the corrections performed separately as well as combined. To avoid an influence on the angle dependency by combination of the horizontal and vertical calculations for the tissue discrimination, the investigations will be performed for both horizontal and vertical directions separately.

Material and Methods

Using a Kretz Combison 330 ultrasound scanner and a 7.5 MHz bi-plane transrectal probe (VRW77AK), images of tissue mimicking phantoms were recorded. To exclude differentiations by speckle statistics and equipment noise, a series of ten images was recorded and the parameter values in these images were averaged. For the investigation of the depth dependency, a series of images from a commercially available phantom was recorded. This is a homogeneous, isotropic, multi purpose tissue mimicking phantom[1] (see discussion). The ultrasound probe was placed in a fixture adjacent to the phantom material and images were recorded. The control settings on the scanner, as well as the settings for the calculations of the parameter values, were equal to the ones for the clinical application (Huynen et al. 1994).

Angle:

Because the phantom material, used for the investigation of the depth dependency, could not be imaged in the total region of interest for the examination of angle related dependencies, a mixture of 80% Shell Multigrade motor oil and 20% Arachidus (peanut) oil was used, with the same ultrasound velocity as soft tissue. The statistical speckle characteristics of this mixture are different from the ones for

---

[1] Model 84-317, RMI, Division of Physics Associates Limited
PO Box 327, 7617 Donna Drive, Middleton, WI 53562, USA

human prostate tissue, but the angle-related dependency of the co-occurrence parameters is caused by the rotation of the ultrasound beam, instead of these speckle characteristics. The ultrasound probe was placed inside the material and 10 images, displaying the total region of interest (>180° Transverse, 100° Longitudinal), were recorded. The parameters were calculated at a fixed distance, for 256 angles from 0 to π radian, and averaged for all the images. The co-occurrence matrix was calculated in orthogonal directions, corresponding to the pixel structure of the image. To examine a possible method to circumvent the dependencies on the angle of the scan lines in the image, the computations were also done in directions parallel and perpendicular to the scanning direction of the ultrasound beam (polar coordinates).

Distance:

To investigate the depth dependency of the parameters, a series of ten images of the tissue mimicking phantom was used. The parameters were calculated between 1 75 cm and 4 cm from the ultrasound probe, along a straight ultrasound scan line. The ultrasound probe is situated in the middle, at the bottom of the image, or just below. By analyzing a vertical line in the image, through the centre of the probe, one ultrasound scan line is used, and no angle dependencies are encountered. Similar as for the angle related investigations, the parameter values were averaged for the different images. Because the depth dependency is correlated to the size of the ultrasonic speckle (Oosterveld et al. 1995), the influence of increasing window size was investigated as well as increasing inter-pixel distance for the construction of the co-occurrence matrix. From these investigations, however, it could be concluded that no pre-processing correction could be achieved, using these two settings (see results/discussion). Because these pre-processing corrections could not eliminate the depth dependency, a post-processing correction was applied as described by Morris (1988). In images of the phantom material, regression curves to describe the relation between the parameter values and the distance to the ultrasound probe were determined. After calculation of the parameter values in images of the prostate, these regression curves were used to correct the parameter values for the depth dependency. These corrected parameter values were used in the classification process of the visualized tissue histology.

Grey value statistics

During the investigation of the angle dependencies, a stepwise deviation could be noticed, caused by the sparse filling of the co-occurrence matrix (see results). To avoid this deviation, the calculations were also performed with the grey values compressed. This compression was done by normalising the grey values for the mean and the standard deviation.

Tissue classification:

After the investigations for the position dependencies using the images of phantom material, the results were applied to the material used in the automated tissue classification process. The retrospective classification results of the 331 biopsy

	Normalised		
	D^2	D	Constant
Uniformity	-0.0006	0.004	-0.0018
Contrast	16.8619	-92.249	140.417
Inv.Dif.Mom.	-0.082	0.4653	-0.3607
Entropy	0.1216	-0.7896	7.026
SNR	-	-	-

	Ordinary		
	D^2	D	Constant
Uniformity	0.0012	-0.006	0.0079
Contrast	-251.35	1234.99	-473.1
Inv.Dif.Mom.	0.0126	-0.0564	0.1038
Entropy	-0.1598	0.7779	6.5684
SNR	-0.0395	0.0432	2.5237

Table XII *The regression equations of the depth dependency for the different parameters in normalised as well as ordinary phantom images* $Par = aD^2 + bD + Constant$ *Because the SNR is constant in normalised images, no regression could be calculated*

specimens with benign or malignant tissue histology were investigated using the corrected parameter values. The results in the phantom material indicated the use of a pre-processing modification in the parameter calculations for the angle dependency and a post-processing correction for the depth dependency The pre-processing and the post-processing were investigated separately and together.

Results

Angle:

As an example, the results are only presented for the parameter Entropy. The dependencies for the other parameters were similar. In Figure 7 the angle dependency is presented, with the calculations performed in the horizontal direction. For the co-occurrence matrix constructed in the vertical direction, a similar dependency was found with a phase shift of $\frac{1}{2}\pi$. Because the dependencies for horizontal and vertical

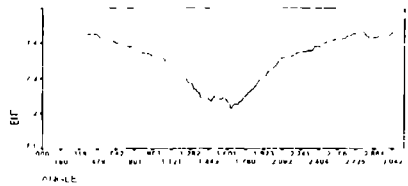

Figure 7 *The Entropy as function of the angle in the image, in normal images. The co-occurrence matrix is constructed in the horizontal direction.*

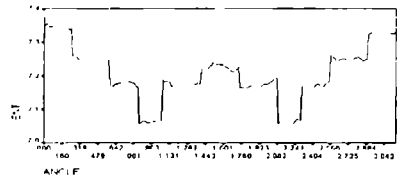

Figure 8 *The Entropy as function of the angle, in normal images. The matrix is constructed perpendicular to the scan lines.*

Figure 9 *The Entropy as function of the angle in a normalised image, with the co-occurrence matrix in the horizontal direction.*

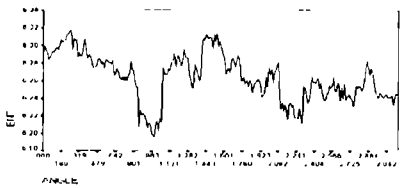

Figure 10 *The Entropy as function of the angle in a normalised image, with the calculations performed perpendicular.*

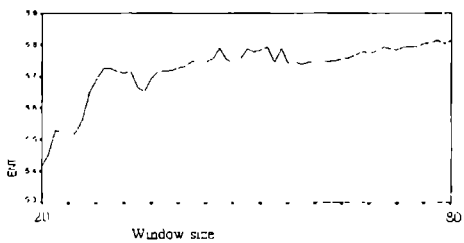

Figure 11 *The influence of the window size for the construction of the co-occurrence matrix on the Entropy, calculated at a fixed position.*

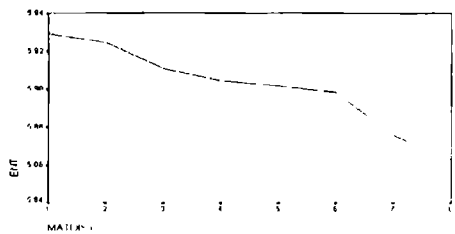

Figure 12 *The influence of the inter pixel distance for the construction of the co-occurrence matrix on the Entropy, calculated at a fixed position.*

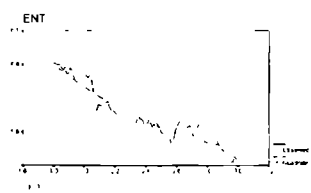

Figure 13 *The Entropy as function of the distance to the transducer, and the calculated regression curve.*

Correction	Sens	Spec	ROC-d
None	75.5	72.9	34.2
Angle	68.6	72.5	29.1
Distance	70.6	73.4	31.1
Both	74.5	76.0	35.7

Table XIII *The influence of the correction algorithms on the classification results.*

calculations are similar, the subsequent investigations are only performed for the horizontal direction.

Figure 8 shows the dependency of the Entropy to the angle in a normal ultrasound image, when the direction in which the co occurrence matrix is constructed is rotated perpendicular to the ultrasound scan line The sampling of the video image takes place in a rectangular grid. In this way the vector for the construction of the co occurrence matrix can not be rotated exactly similar to the ultrasound scanning direction. Together with the sparse filling of the matrix, this causes the stepwise deviation in Figure 8 This stepwise deviation is also found for the Uniformity, but not for the other parameters The sparse filling of the matrix is caused by the large number of grey tones (256) used in combination with the relative small (30 x 45 pixels) Region Of Interest (ROI) for the matrix-construction The co-occurrence matrix is filled maximally for only ± 2 % (ROI / 256^2). To avoid deviations by this sparse filling, all following calculations are done on compressed images and the number of grey tones is reduced to 32. The number of grey values must be kept as large as possible to reduce any information loss. With 32 grey values, the matrix can be filled for 100% To exclude the influence of the first order grey tone statistics as well, the images are normalised for the mean and standard deviation of the grey value The grey values of the pixels (in the window in which the co-occurrence matrix is calculated) are transformed to yield a mean grey value of 16 with a standard deviation of 8 Values above 31 or below 0 are clipped Figure 9 and Figure 10, respectively, show the Entropy as function of the angle in a normalised image without and with the angle correction.

Distance:

Figure 11 shows the influence of the window size for the construction of the co-occurrence matrix, Figure 12 shows the same for the distance between neighbouring pixels in this construction In combination with Figure 13, these figures show that neither the window size nor the inter-neighbouring pixel distance have enough influence on the calculations to be used to correct the parameter values for the depth dependency Therefore, a post-calculation correction is applied Regression curves of the depth dependency of the parameter values are calculated (see Table XII) and afterwards used to correct the calculated parameter values

Figure 14 shows the parameter values for the Entropy in a homogeneous ultrasound image when no corrections are performed. In Figure 15 both corrections are performed and a more uniform distribution of the parameter values can be seen In Figure 15, however, a different grey scale is used to emphasize the small variations in the entropy values. Using the same scale, Figure 15 would present a uniform region of grey values, in which no distinction between the different entropy values could be noticed.

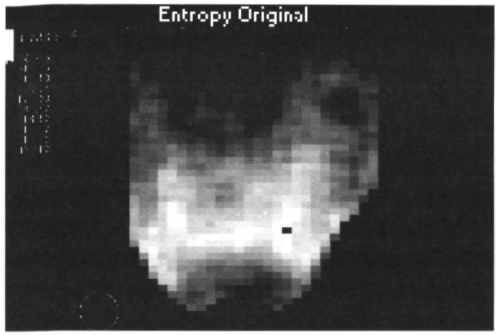

Figure 14 *The Entropy in an ultrasound image of phantom material, without any corrections performed.*

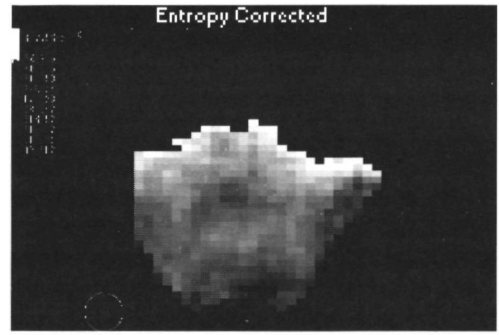

Figure 15 *The Entropy in an ultrasound image of phantom material, with the angle and depth corrections performed.*

Tissue discrimination:

Table XIII shows the results of the tissue classification with and without corrections. For the classification of tissue samples, however, the normalisation turned out to be disadvantageous and was, therefore, omitted. The regression curves for the correction of the parameter values are correspondingly determined in phantom images without pre-processing the grey values. By performing both corrections, an increase in overall classification results can be seen. This increase is caused by an increase in specificity, while a small decrease in sensitivity can also be seen.

Discussion and Summary

Phantom material:

During this study, phantom material is used to represent homogeneous isotropic tissue: a liver tissue phantom for the depth dependency examinations and an oil mixture for the angle dependency. Because the angle related problems are caused by the rotation of the single element transducer instead of the tissue related ultrasound characteristics, the use of this phantom material is legitimate. The depth dependency, however, may be influenced by the tissue properties and these properties may differ between liver and prostate tissue. The increase in overall classification results, using the liver tissue mimicking phantom material to derive the regression curves, justifies the use of this material for the correction of the depth dependencies. It may be concluded that the dependencies, caused by the physics of the ultrasound beam, are not influenced by the visualized material, or that these properties are similar for liver and prostate tissue.

Grey tone statistics:

Morris (1988) determined a post-processing correction for the distance dependency of co-occurrence parameters in ultrasonic images of the human placenta.

During this investigation, a strong dependency was found between the parameters and the absolute grey value. Therefore, the mean grey value in these images was normalised by linear transformation. The co-occurrence parameters, however, are not dependent on linear transitions of the grey value, but on amplifications. To decrease the dependency on the grey values, it would be better to normalise the images for the mean and the standard deviation of the grey values. Because the SNR is an important parameter in our tissue discrimination algorithms, however, this normalisation is disadvantageous and, therefore, omitted.

Angle:

During a pilot study, the combination of horizontal and vertical calculations yielded the best classification results when compared to the use of only one direction. A possible explanation is the (small) averaging of the two directions. Comparison of Figure 7 and Figure 9 shows that the dependency on the angle is similar for normalised and original images. The correction of the angle dependency, however, can be improved markedly by the normalisation (and compression) of the grey values in the images The dependency after normalisation and correction not only disappeared almost totally, but also a decrease can be seen in the range of the variation in the parameter values (see Figure 10).

Distance; pre-processing:

The dependency of the parameters on the distance between the echo probe and the calculation position seems to be related to the local speckle size. Therefore, it is expected that the window size and the inter-pixel distance for the co-occurrence matrix construction can be used for the correction of this dependency. The graphs in Figure 11 and Figure 12 show that these two parameters only have small control over the values of the parameter calculations Figure 13 shows that the range of the parameter value is larger than the influence of the control settings and it can be concluded that these settings do not have enough influence on the calculated parameter values to be used as 'pre-processing' correction for the dependency of the parameter values on the distance to the ultrasound probe. Furthermore, only the window size shows the expected increase in parameter values, whereas the inter-neighbouring pixel distance shows an opposite influence A possible explanation can be given by the total information used (read: number of grey tone transitions used for the construction of the co-occurrence matrix), if the inter-pixel distance increases, less information is used for the construction of the co-occurrence matrix. On the other hand, if the window size for the construction increases, more information is used for the construction of the matrix. In this way the total number of grey tone transitions, used for the construction of the co-occurrence matrix, has influence on the parameter outcomes, independent of the method of changing this number. This explanation is also valid for the depth dependency of the Entropy; with increasing distance between the analysis location and the ultrasound transducer, the resolution of the received echo signal decreases, together with the information density. Parallel to the decrease of the Entropy with decreasing information in Figure 11 and

Figure 12, the parameter values decrease with increasing distance to the ultrasound probe.

Distance; post-processing:

For his depth dependency measures, Morris used a linear array transducer. We use a 7.5 MHz transrectal single-element scanning transducer. This transducer measures not only dependency caused by the physics of the ultrasound, but also dependency caused by the diverging pattern of the scan lines. The scan lines spread with distance and this phenomenon can cause another depth dependency The regression analysis of the depth dependency, however, showed similar (second order) dependencies for the single element transducer as were found by Morris for a linear array transducer. The depth dependencies introduced by the spreading of the scan lines has no significant, or similar influence as caused by the physics of the ultrasound beam. The post-processing corrections are only valid for a limited part of the ultrasound image. This part, however, is sufficient for the analysis of prostate images.

Tissue discrimination:

The values in Table XIII show that the position dependent corrections slightly improve the classification results when used in combination. If one of the corrections is applied independently, the results decrease. These classification results are calculated in a group of puncture biopsy samples. In this group, a correlation exists between the angle in the image and the distance between the biopsy location and the ultrasound probe, due to the fixed line in the images along which the biopsies are taken. This correlation between angle and depth for the biopsies can cause the decrease in the classification results if only one of the corrections is performed. The combination of the corrections, however, shows an increase in the classification results for the automated interpretation of ultrasound images of the prostate. This increase is caused by an increase in specificity, accompanied by a decrease in sensitivity. The classification of benign tissue improves, while the detection of carcinoma decreases. The phantom material mimics the appearance of benign tissue and the derived correction algorithms are better for benign tissue. Because the total classification gain is small and the sensitivity for cancer detection is more important than the specificity, one can argue that the corrections are not necessary.

Conclusion

Angle:

The angle dependency of the speckle pattern in images, constructed with single element ultrasound transducers, can be avoided by rotating the vector for the construction of the co-occurrence matrix perpendicular to the scan lines. If the grey values in the images are compressed, deviations from the sparse filling of the co-occurrence matrix are avoided.

Distance:

Similar to the methods and results presented by Morris, second order regression curves can be determined in phantom material for post-processing correction of the parameter values to eliminate the depth dependency for prostate images.

Tissue discrimination:

For the tissue discrimination, the correction algorithms increase the specificity for cancer detection in the set of biopsy samples. This increase is at the cost of the sensitivity. The normalisation and compression of the grey values, introduced to enhance the angle corrections, is disadvantageous for the classification results because the SNR is an important parameter for the tissue discrimination.

Chapter VIII

FUTURE DEVELOPMENTS

3-Dimensional calculations and presentations

At the moment, a study is being performed, investigating the predictive diagnostic value of ordinary TRUS, computer analyzed TRUS images, and Magnetic Resonance Imaging (MRI). This study gives us insight in the diagnostic value of each imaging modality. Transverse prostate images are recorded (using TRUS as well as MRI) every 4mm, before the gland is removed with radical surgery. The removed gland is cut into slices of 4mm and every slice is analyzed by a pathologist. After pathologic analysis, the tissue histology of the entire gland is known This pathologic information is used as the gold standard of the tissue histology and compared to the different imaging modalities. The consecutive images are interpreted and regions with presumed prostate carcinoma are marked. For all the modalities, a 3-dimensional model is constructed After fitting the different models, a comparison between the tissue histology and the image interpretation is made according to tumour localisation and size.

The information about the prostate obtained with ultrasound is a 3-Dimensional (3D) data set, representing the entire gland Until now, only 2-Dimensional (2D) information extracted from this data set has been used. The results from the calculations on this information were also presented in a 2D way (segmented and/or analyzed ultrasound images) It is possible, however, to use the full scale of 3D information. The segmentation, as well as the texture quantification algorithms can be extended to operate on the 3D information set. This extension will increase the computational load and the additional value, achieved with this extension, is yet unknown. It is less complicated to perform the calculations on the 2-dimensional images and to use all results to construct a 3-dimensional view of the gland. Figure 16a to Figure 16f present a projection of a 3D reconstruction of the prostate. The contours are determined using the filter-algorithms as described in Chapter II By applying these filters to all images of consecutive cross-sections, a segmentation of the entire prostate is obtained. The consecutive contours are connected, by drawing lines between the points of two successive contours, forming triangles. After triangulation of the contours, an observers view is constructed by calculating the linear perspective of the triangulated shape. Figure 16a to Figure 16f present a series of projections with different viewing angles. With an on-line computer screen, this information can be shown in a more comprehensible way. By displaying a rotating object and/or applying stereo vision, the entire 3-dimensional information can be visualised. The example, presented here, used images with an intermediate distance of 4mm. By increasing the resolution, or using sophisticated algorithms, like interpolation, shading, and/or ray-tracing, a smoother, more realistic view of the prostate is given. With this 3-dimensional presentation, more knowledge and detail about the shape and symmetry of the gland can be obtained. It demands, however, another way of viewing and interpreting information. Besides the presentation of the shape, it is also possible to project information about the structures inside the prostate. With dedicated software, the shape information can be projected translucent

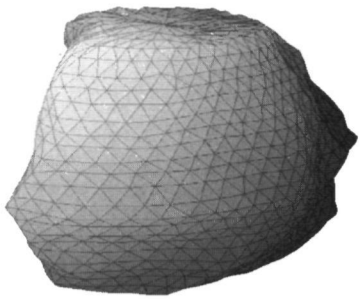

Figure 16a

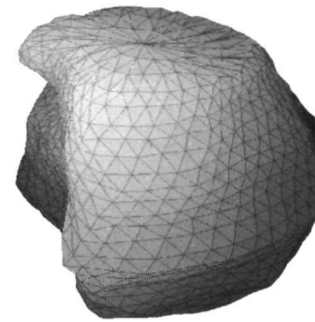

Figure 16b

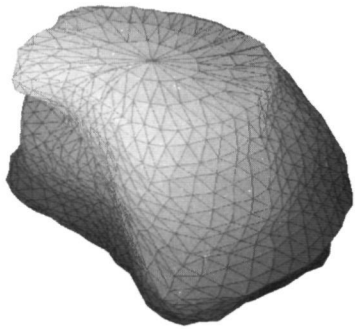

Figure 16c

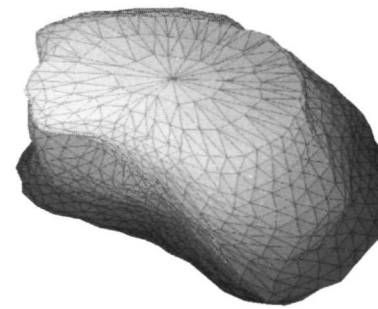

Figure 16d

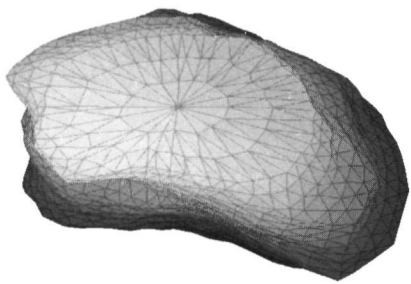

Figure 16e

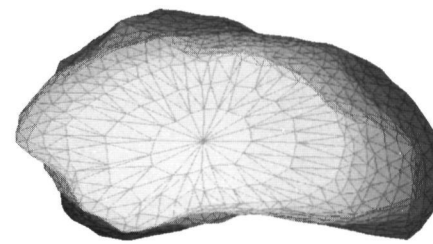

Figure 16f

Figure 16a to Figure 16f *Two-dimensional projections of a three-dimensional constructed prostate view, with different viewing angles.*

and information from the interior of the gland, like echo-structure, anatomic information, or areas with increased probability of malignancy, can be visualised.

Combination of automated analysis and clinical diagnosis

For the prediction of tissue histology, only the ultrasonographic texture parameters of the images are used. Clinical parameters (DRE, PSA, and/or TRUS) also contribute to the information about the histology of the gland and incorporation of this information into the tissue discrimination algorithms will probably improve the classification accuracy. By extending the samples, containing the textural information of the biopsies, with the clinical parameters DRE, PSA, and TRUS interpretation, a decision tree constructed for tissue discrimination will automatically determine the usefulness of these parameters and, if necessary, integrate them into the decision process

Table XIV presents the classification of benign, malignant, and inflamed prostate tissue with the addition of serum PSA levels and local mean grey value of the ultrasound image. The classification is performed on a subset of the biopsies and no majority vote is applied on the biopsy samples. Furthermore, the categorization is performed retrospectively and no optimal prospective classification is determined with cross validation The samples are split into two subsets, one (containing ⅔ of the samples) for the construction of the decision tree and one (with ⅓ of the samples) for a prospective evaluation. The example serves only to illustrate the improvement achieved by using clinical as well textural parameters. Comparable to the results found in Chapter VI, the sensitivity is low, especially for the malignant and inflamed tissue samples With the addition of clinically relevant information, the retrospective as well as prospective classification results improve markedly. In the decision tree, the PSA value and the mean grey level in the analysis region were incorporated. The findings on Digital Rectal Examination, as well as the human interpretation of the ultrasound images, did not provide useful information. By using the clinical information, the retrospective accuracy for this example improved from 79 5% to 90.0%, while the prospective accuracy showed an improvement from 47 6% to 76.0%.

The problem of the inclusion of clinical parameters is that the majority of the decisions, made for the classification, are taken without any image processing information; only the PSA levels are evaluated This means that this technique can not be used to colour code images or to mark biopsy locations, because the PSA levels are not related to the ultrasound image A possibility to circumvent this drawback would be the use of clinical parameters, not related to the images, in levels of the decision tree near the external nodes In this way, the significant decisions will be based on the image processing parameters and differentiation of the image regions according to assessed tissue histology is possible. Next, the clinical parameters are used for the adjustment of the calculated probabilities for malignancy. In this way,

Retrospective (n)	Sensitivity	Specificity
Benign (271)	89.7 [87.5]	79.6 [94.2]
Malignant (114)	73.7 [88.6]	89.3 [93.5]
Prostatitis (112)	60.7 [100]	96.1 [97.7]
Prospective		
Benign (134)	67.9 [87.5]	48 2 [78 6]
Malignant (57)	28 1 [88.6]	81.0 [85 2]
Prostatitis (55)	18.2 [96.4]	81 7 [96.3]

Table XIV *The retrospective classification results with only the textural parameters and [with the inclusion of PSA levels and average grey level]*

regions, suspected for malignancy, can be marked, while the actual probability of prostate carcinoma can be calculated with the use of the additional clinical knowledge.

Early detection of prostate cancer

The research described here, used the information of histologically proven prostate cancer. There are indications that malignancy in the prostate is preceded by so called premalignant changes in the tissue like atypical (primary) hyperplasia, dysplastic hyperplasia, and intraductal dysplasia (Schulze, 1991). It is, however, still unknown how and why these changes evolve into prostate malignancy. Once this pathogenesis of prostate cancer is known and if these histological tissue changes produce measurable texture changes in the ultrasound images, it should be possible to detect malignant prostate tissue before the tumorous growth occurs. This would be highly beneficial for patient healthcare and for the reduction of morbidity and mortality from prostate cancer.

Treatment of prostate cancer

Until now, the methods described in this thesis are only used for the detection of prostate cancer during the diagnostic stage. However, they might also be applicable during and after treatment. By quantification of the area involved in tumour-spreading, local treatment, like brachytherapy, cryosurgery, implementation of thermal seeds,

and high intensity focused ultrasound, can be restricted to the malignant tissue area, not damaging the surrounding benign tissue. Also for the evaluation of non-surgical treatment, the quantification of tumour-involved tissue is useful. However, probably all tissue is influenced by the treatment and may not display the same textural features as before therapy. Before the quantification of tumour-spreading can be applied and used to control and evaluate local therapy, the automated interpretation of the ultrasound images has to be evaluated for the quantification of tumour volume as described at the beginning of this chapter.

Surpassing ultrasonography of the prostate

The methods described in this thesis are not specifically designed for ultrasonography or for the analysis of prostate images. However, some information is specific for the analysis of ultrasonographic prostate images. For the segmentation of the images, information about the expected shape and ultrasonographic appearance of the gland is used and, during the training phase of the tissue discrimination algorithms, the tissue histology of benign and malignant prostate tissue was used. By replacing this specific information, the algorithms can easily be adapted to other imaging modalities, or adjusted for the interpretation of images of other organs. It may also be possible, by extending the parameter set, to discriminate between other histology types within the prostate. When applying TransUrethral Microwave Thermotherapy (TUMT) a large variation in treatment success can be seen. This difference in treatment effect is probably caused by different rates of epithelial and stromal tissue in the gland. If an automated system can distinguish the ultrasonographic texture of these tissue types, the treatment success can be predicted and, therefore, the treatment can be made more specific for each patient. With the texture quantifying parameters, used for the detection of carcinoma, we were not able to distinguish epithelial from stromal prostate tissue, or to discriminate benign, malignant, and inflamed prostate tissue simultaneously, but this can also be caused by the optimisation process for the detection of prostate cancer (see discussion Chapter VI).

Colour coding of the images

In the external nodes of the decision trees, the conditional class probabilities are calculated proportionally to the relative class frequencies in each node. These class probabilities give an indication about the likelihood of prostate carcinoma to be present. There is no indication, however, about the relevance of this prediction. By looking at the probability of a sample to reach the external node in which the class was assigned, an assessment of the significance of the predicted tissue histology can be obtained. Also the level in the tree of the external node, i.e. the number of decisions necessary to make the classification, can be used as an assessment of the

classification significance. Problem of these calculation is the need to combine two values (probability of malignancy and significance of prediction) into one colour for coding the images. This can be resolved by using the Hue-Saturation-Intensity (HSI, also called Hue-Saturation-Lightness) coding for the colours to be used. This colour coding method resembles the human perceptual system, but can easily be transformed to the Red-Green-Blue (RGB) coding, used in computer imaging. The tissue histology can be presented with the hue (≡colour), while the saturation or the intensity can be used to represent the significance.

Artificial Intelligence

The information used for automated interpretation of the ultrasound images is used in a straightforward way. It is, however, also possible to combine the textural classification with the segmentation knowledge Lee et al. (1985) reported the ultrasound texture of prostate carcinoma to be the same for malignancy confined to the gland and cancer penetrating the prostate capsule. Using this knowledge, the texture descriptions of regions outside the segmented prostate area, can give an indication about capsular penetration Also the localisation of prostate cancer near the capsule can give an indication about capsular involvement. The difference of ultrasound texture inside and outside the gland could be used to improve the boundary detection algorithms and several segmentation methods, based on image texture, are implemented (Hsiao and Sawchuk, 1989; Vistnes, 1989). Du Buf et al. (1990) evaluated the use of textural features for the segmentation of images and the Haralick parameters were among the best performing methods. Haddon and Boyce (1990) presented a segmentation algorithm, based on the co-occurrence matrix. In this way, the segmentation output is based upon the textural quantification values instead of used for the limitation of the calculation area. Prater and Richard (1992) used feedforward neural networks to segment ultrasound images into prostate and non-prostate regions. The networks were trained with images segmented by an experienced sonographer. The use of textural information, however, can disturb the segmentation if the carcinoma is invading the peri-prostatic area.

By implementation of an Artificial Intelligent (AI) system, the combination of segmentation and textural information can be achieved. In such a system, not only textural information and grey level statistics would be used, but also structural knowledge and con-textual data. Segmentation information could be used to gain knowledge about regularity and symmetry of the gland. Localisation of textural information can be combined with anatomical knowledge. Integration of interpretation data, clinical information, test results, and patient history with urological expertise can, besides diagnosis, provide suggestions about treatment

Chapter IX

SUMMARY AND CONCLUSION

Summary

This thesis presents methods for the automated interpretation of ultrasonographic prostate images Due to the lack of accuracy, objectivity, and reproducibility, the interest in ultrasound as imaging modality for the prostate is decreasing Two important clinical aspects of visualisation of the prostate are segmentation and texture discrimination Segmentation is performed to obtain the volume of the gland, an important parameter for patients with benign enlargement Texture discrimination is used to distinguish between different tissue types, essential for patients, suspected to have a malignancy

The possibility to improve volume determination and simultaneously reduce the ultrasound investigation time, encouraged us to implement an automated method for the segmentation of the prostate images Using fast implementations of linear filters, all edges in the images are detected With knowledge of the expected shape and ultrasound appearance of the prostate, the correct edges are enhanced and selected and with adaptive interpolation, the prostate boundary is produced Constructed and evaluated for volume determinations in the gland, this method is highly accurate and reproducible and can save a lot of investigation time during routine TRUS examinations Patient comfort is increased by the reduced investigation time For the tissue discrimination algorithms, the segmentation is used to restrict the Region Of Interest for the texture quantification and the interpretation of the colour coded images is facilitated, because only the prostate region itself is analyzed

Benign and malignant tissue have different ultrasound characteristics and will, therefore, be visualised differently with ultrasound The ultrasonographic image texture of benign tissue will vary from the one for malignant tissue Human perception, however, is not capable of retrieving all available information from the ultrasound images The inability of a human observer to utilise all the information present and the possibility of an automated method to visualise this information yields a perfect combination for the automated interpretation of ultrasonographic image texture The texture can be used to classify the displayed tissue Texture quantifying parameters are presented, originally designed for the analysis of areal photographs These parameters seem also valid for the classification of the histology of visualised prostate tissue in ultrasonographic images of the gland Tested for the classification of ultrasound images of puncture biopsies, these parameters show good discriminating power between benign and malignant prostate tissue Using a binary decision tree, the feature vector, formed by the texture parameters, is classified according to the majority of histology classes of biopsy samples displaying similar texture features By using a decision tree, a non-parametric classification algorithm is available, which adapts itself to the decision problem and the samples presented during the training phase

In the select population of patients undergoing puncture biopsies, the tissue classification algorithms show good results, especially for the biopsies with negative outcome for some of the clinical diagnostic tests. Clinical diagnosis is based on Digital Rectal Examination, Prostate Specific Antigen levels, and TransRectal UltraSound. The clinical tests, however, have low sensitivity, resulting in high incidental carcinoma rates. With new, non-invasive, therapies for Benign Prostatic Hyperplasia, the exclusion of incidental carcinoma is very important. The prospective classification results for the total patient population are calculated using the values of incidental carcinoma and biopsy rate as found in our urology clinic. When the results for cancer detection are extrapolated to the patient population with prostatism complaints, sensitivity of the automated method is 2.6 times as high as for the clinical diagnosis. The higher sensitivity is accompanied by an increased biopsy rate, resulting in lower specificity. The overall classification of prostate tissue, calculated with the Receiver Operating Characteristic, was 2.5 times higher for the automated method.

Because other tissue types, except from benign and malignant, can occur in the prostate, the tissue discrimination algorithms, developed to distinguish between benign and malignant tissue, may be unsuitable in a clinical application. The application of the decision tree algorithm was, therefore, extended to classify more than two tissue types. The predominant additional tissue type in prostate diagnosis is inflamed tissue (prostatitis) and the algorithms were evaluated incorporating biopsies with this tissue type. Combinations of malignant, benign, and inflamed prostate tissue (prostatitis) were classified, as well as these three histology types together. The results did not change when benign and inflamed tissue were combined into one tissue type (non-malignant). If malignant tissue was combined with prostatitis, to represent deviation from benign tissue, the classification results decreased. With the texture parameters and decision tree algorithm, as used in our research, we were not able to classify the three tissue types. The inability to distinguish between benign and inflamed prostate tissue is probably caused by a large overlap between the two tissue types in pathologic appearance, resulting in similar ultrasonographic texture. The optimisation of the texture related calculation for the discrimination between benign and malignant tissue can also be a determining factor in this problem. Because the addition of prostatitis samples to the benign group did not change the overall classification results and even improved the sensitivity for cancer detection, the methods are also applicable during routine prostate examinations.

The use of ultrasound for the visualisation of the prostate has the disadvantage that the physics of the method produce inhomogeneous images. The attenuation and the interference patterns of the back-scattered ultrasound waves yield a depth dependency in the image texture. The use of a single-element rotating transducer produces an angular dependency. By performing the calculations in polar coordinates, the angle dependency can be reduced. We could not find pre-processing steps for the reduction of the depth dependency. After measuring the depth dependency in tissue

mimicking phantom material, the regression curves of this dependency were used to correct the parameter values, found in prostate images, afterwards The use of only one of the two mentioned corrections, showed a decrease in classification results for the puncture biopsies. This can be caused by the correlation between the angle in the image and the distance between the analysis region and the ultrasound transducer This correlation is caused by the puncture guidance with ultrasound, forcing the biopsies to be taken along a fixed line in the images If both corrections are performed, the overall classification results increase, caused by a large increase in specificity, together with a slight decrease in sensitivity. The decrease in sensitivity could be caused by the phantom material, only mimicking the ultrasound characteristics of benign tissue

Finally, some recommendations and ideas for the near future are presented. A three dimensional presentation of the prostate is given, by combination and projection of the two-dimensional contours, obtained with the automated segmentation. Also, a combination of the texture quantification parameters with ordinary clinical parameters (PSA level and ultrasound grey value) for the detection of prostate carcinoma is given By incorporating the clinical parameter into the tissue discrimination algorithms, accuracy for the classification of biopsy tissue improves This, however, is disadvantageous for the colour-coding of complete TRUS images and especially the identification of possible biopsy locations, because the clinical parameters are prostate specific (global) instead of image specific (local) and, therefore, equal for all image parts.

Conclusion

With automated interpretation, a method is available for accurate and reproducible segmentation of ultrasound images into prostate and surrounding tissue and for representation of tissue histology in the images. Automated volume determination is fast, accurate, and reproducible and ultrasonographic investigation time is reduced. Textural information can be visualised, which is not always perceptible by a human observer In this way, a substantial improvement can be achieved for the interpretation of ultrasound images. The algorithms are incorporated in a clinical application with data management and removable mass-storage media All patient information is readily available and all recorded images of a patient are stored and accessible for monitoring and follow up With the segmentation and tissue discrimination algorithms, the two major applications of ultrasound for the diagnosis of prostatism complaints are automated. Tissue discrimination is especially useful if the ultrasound images show no visually perceptible texture regions suspected to be produced by malignancy The ultrasonographic texture, however, between benign and malignant tissue differs and this difference can be used by a computerized method, to distinguish the two tissue types The areas with increased probability of

malignancy can be marked by colour-coding and puncture biopsies can be guided to these areas.

Samenvatting

Dit proefschrift beschrijft methoden voor de automatische interpretatie van echografische prostaatbeelden Na het initiele enthousiasme over het gebruik van transrectale echografie voor de diagnose van prostaatklachten, is de huidige opinie sterk getemperd. Echografie mist de nauwkeurigheid, objectiviteit en reproduceerbaarheid, nodig voor klinische toepassingen Dit wordt hoogstwaarschijnlijk veroorzaakt door de gebreken van visuele perceptie: menselijke onderzoekers zijn niet in staat om alle informatie in een echobeeld te gebruiken voor de interpretatie ervan. De twee klinisch meest relevante toepassingen van echografische prostaatonderzoeken zijn volumebepaling en weefseltypering Het volume van de prostaat is een belangrijk diagnostisch gegeven bij patiënten met een goedaardige prostaatvergroting. Weefseltypering is belangrijk als er een verdenking voor de aanwezigheid van prostaatkanker is.

De meest nauwkeurige methode voor volumebepaling van de prostaat is planimetrie. Op vaste afstanden wordt een transversaal echobeeld opgeslagen. In elk beeld wordt de contour van de prostaat getekend en het oppervlak berekend dat wordt omsloten door deze contour. Door de oppervlakken van alle beelden bij elkaar op te tellen en te vermenigvuldigen met de afstand tussen de opeenvolgende beelden, kan het prostaatvolume berekend worden. Het grote nadeel van deze methode is de tijdsduur, nodig voor het intekenen van alle contouren. Door de contourdetectie in de beelden te automatiseren, hebben we een snelle en nauwkeurige methode om het analyse gebied voor de weefselkarakterisering te bepalen. Door deze methode tijdens de clinische onderzoeken te gebruiken voor de prostaatvolume-bepaling, wordt de nauwkeurigheid hiervan verbeterd en tegelijkertijd de onderzoekstijd ingekort

Benigne (goedaardig) en maligne (kwaadaardig) prostaatweefsel hebben verschillende echografische kenmerken en deze kunnen, hoewel ze niet altijd zichtbaar zijn, door een computersysteem gebruikt worden voor de differentiatie van het weefsel. De echografische structuren worden beschreven door textuur parameters, oorspronkelijk ontwikkeld voor de analyse van luchtfoto's. Ook voor de splitsing van echobeelden van benigne en maligne prostaatweefsel zijn deze parameters geschikt. De scheiding tussen de textuurkenmerken van beide weefseltypes gebeurd m b.v. een binaire beslisboom. Hierdoor hebben we een non-parametrisch classificatie algoritme, dat zichzelf aanpast aan het specifieke classificatie probleem en aan de populatie, gebruikt gedurende de leerfase van het systeem.

Voor de patienten waarbij prostaatbiopten zijn genomen, zijn er met de weefseltyperings algoritmen goede resultaten geboekt, vooral voor de sub-populaties waarbij een of meerdere klinisch diagnostische tests negatief waren. De klinische diagnose is gebaseerd op het rectale toucher, de hoogte van het Prostaat Specifiek Antigeen, en de resultaten van het echografische onderzoek De klinische diagnose heeft echter een erg lage sensitiviteit, waardoor er veel kanker gemist worden. Door de nieuwe,

niet-invasieve behandelingsmethoden voor Benigne Prostaat Vergroting, is er bij deze patiënten geen weefsel beschikbaar voor pathologische analyse. Het is daarom belangrijk om bij deze patiënten de aanwezigheid van kanker uit te sluiten. Uitgaande van de klinisch gevonden percentages biopten en incidenteel carcinoma bij de niet gebiopteerde patiënten zijn de classificatie resultaten van de automatische methode vergeleken met de klinische diagnose. Voor de totale patiënten populatie met prostaatklachten is de sensitiviteit voor kankerdetectie 2,6 keer zo hoog voor de weefseltypering d.m.v. automatische beeldanalyse. Deze verbeterde detectie gaat gepaard met een hoger aantal biopten, resulterend in een lagere specificiteit. Met de Receiver Operating Characteristic kan de classificatie in zijn geheel getest worden, en hieruit blijk dat de automatische methode twee-en-een-half keer zo goed is als de klinische diagnose.

Omdat er behalve benigne en maligne weefsel ook nog andere weefselsoorten kunnen voorkomen in de prostaat, is het niet zeker of de weefseltypering, gebaseerd op het verschil tussen benigne en maligne weefsel, ook geschikt is voor de classificatie van echografische prostaat beelden zoals ze in de praktijk voorkomen. Derhalve hebben we de beslisvormingstechnieken uitgebreid, om ook in staat te zijn meerdere weefseltypes tegelijk te 'herkennen'. Omdat ontstekingen in de prostaat (prostatitis) de meest voorkomende 'extra' weefselsoort is, hebben we dit weefseltype meegenomen in de classificatiealgoritmen. Zowel combinaties van benigne, maligne en ontstoken weefsel zijn geclasseerd alsook de drie weefselsoorten apart. De combinatie van de niet-maligne weefselsoorten (benigne en prostatitis), leverde geen significante verandering in de resultaten op. De combinatie van maligne en prostatitis, daarentegen, zorgde voor een daling in de classificatie. Met de gebruikte algoritmen was het ook niet mogelijk om de drie weefsel types van elkaar te onderscheiden. Er is een grote overlap tussen de histologiën van benigne en ontstoken prostaat weefsel en deze overlap zou terug te vinden kunnen zijn in de echografische kenmerken van deze weefseltypes. Een andere oorzaak voor de problemen in de classificatie kan de optimalisatie van de algoritmen voor het opsplitsen van benigne en maligne weefsel zijn. Omdat de combinatie van benigne weefsel met prostatitis de algehele classificatie niet negatief beïnvloedt, en zelfs de sensitiviteit voor kanker detectie verhoogt, kunnen de weefselclassificatiealgoritmen zonder problemen gebruikt worden voor de classificatie van echografische prostaatbeelden.

Het gebruik van echografie voor het in beeld brengen van de prostaat heeft het nadeel dat, door de fysische eigenschappen, er een niet-homogeen beeld ontstaat. Door interferentie patronen van de teruggekaatste geluidsgolven en verzwakking van het geluidssignaal in het weefsel, ontstaat er een diepteafhankelijkheid in de gemeten textuurparameters. Door het gebruik van een roterende 'single-element' echotransducer ontstaat een hoekafhankelijkheid. Deze hoekafhankelijkheid kan voorkomen worden door de berekeningen in een polair coördinatenstelsel uit te voeren. Voor de afstandsafhankelijkheid kon geen pre-processing correctie gevonden

worden. In materiaal dat de echoeigenschappen van weefsel nabootst, zijn de afstandsafhankelijkheden gemeten, en de regressiecurven van deze metingen zijn gebruikt om de parameter waarden, gevonden voor prostaat biopten, achteraf te corrigeren. Als alleen de hoek- of alleen de afstandscorrectie uitgevoerd wordt, nemen de classificatie resultaten af Dit kan veroorzaakt worden door de positie van de biopten in het beeld· alle biopten zijn langs een vaste lijn in het beeld, nodig voor de echogeleiding van de biopten, genomen en hierdoor ontstaat er een correlatie tussen de hoek en de afstand van de beeldanalyse van de biopten Als beide correctie algoritmen worden gebruikt verbeteren de resultaten, veroorzaakt door een betere classificatie van de benigne biopten, vergezeld door een daling in kankerdetectie Het gebruik van een weefselfantoom dat de echokarakteristieken van benigne weefsel nabootst kan de oorzaak hiervan zijn

Tenslotte zijn enkele aanbevelingen en ideeen voor de nabije toekomst gegeven. Een drie-dimensionale presentatie van de prostaat is gepresenteerd Door combinatie van de twee-dimensionale contouren, gebruikt voor de segmentatie algoritmen, kan een 3-dimensionaal model worden geconstrueerd Door een projectie in perspectief van dit model te bekijken onder verschillende hoeken, is de 3 dimensionale informatie beschikbaar. Ook is de combinatie van beeldbewerkingsparameters met klinische gegevens geevalueerd. Door gebruik te maken van PSA en echodichtheid (grijswaarde) wordt de weefsel herkenning sterk verbeterd. Dit heeft echter het nadeel dat de PSA niet specifiek voor de verschillende gebieden in het echobeeld is, en dus ook niet gebruikt kan worden voor de markering van gebieden met verhoogde kans op prostaat kanker.

Conclusie

Automatische analyse van echografische prostaat beelden, is nauwkeurig en reproduceerbaar. De beelden kunnen gesegmenteerd worden in prostaat en omliggend weefsel. Ook is de differentiatie van het weefsel in maligne en niet-maligne mogelijk Door inkleuring van het echobeeld aan de hand van textuur kenmerken, niet altijd zichtbaar voor het menselijke oog, kan additionele informatie gevisualiseerd worden. Beide algoritmen zijn verenigd in een computersysteem met datamanagement en massaopslagcapaciteit voor de echobeelden. Doordat alle gegevens en de beelden gemakkelijk op te vragen zijn is dit systeem een goed hulpmiddel voor de diagnose en follow-up van patienten met prostaatklachten. De twee belangrijkste toepassingen van echografie voor de diagnose van prostaatklachten zijn hierdoor geautomatiseerd. Het volume kan bepaald worden d.m.v. segmentatie in opeenvolgende echobeelden. Het weefsel kan getypeerd worden m.b.v. textuuranalyse, en gebieden met verhoogde kans op prostaatkanker kunnen gemarkeerd worden en weefselbiopten kunnen gericht uit deze gebieden genomen worden.

REFERENCES

Aarnink R G , Huynen, A L , Giesen, R J B , de la Rosette, J J M C H Debruyne, F M J and Wijkstra H AUTOMATED PROSTATE VOLUME DETERMINATION WITH ULTRASONOGRAPHIC IMAGING
J Urol vol 153 pp 1549 1554 1995

Aus, G , Hermansson, C G , Hugosson J and Pedersen, K V TRANSRECTAL ULTRASOUND EXAMINATION OF THE PROSTATE COMPLICATIONS AND ACCEPTANCE BY PATIENTS
Br J Urol vol 71 pp 457 459 1993

Bertermann, H , Loch T and Gouge, J O COMPUTERGESTEUERTE ULTRASCHALLBILD ANALYSE
Urologie Nephrologie vol 1 pp 24 30 1989

Bostwick, D G Cooner, W H , Denis, L Jones, G W , Scardino, P T and Murphy, G P THE ASSOCIATION OF BENIGN PROSTATIC HYPERPLASIA AND CANCER OF THE PROSTATE
Cancer vol 70 (suppl) pp 291 301 1992

Boyle, P NEW INSIGHTS INTO THE EPIDEMIOLOGY AND NATURAL HISTORY OF BENIGN PROSTATIC HYPERPLASIA In Kurth, K and Newling, D W W editors BENIGN PROSTATIC HYPERPLASIA RECENT PROGRESS IN CLINICAL RESEARCH AND PRACTICE New York Wiley Liss, 1994 3-18

Breiman, L , Friedman, J H , Olshen, R A and Stone, C J CLASSIFICATION AND REGRESSION TREES Wadsworth International Group Belmont California, USA 1984

Chodak, G W , Wald, V , Parmer E , Watanabe, H , Ohe, H and Saitoh, M COMPARISON OF DİGITAL EXAMINATION AND TRANSRECTAL ULTRASONOGRAPHY FOR THE DIAGNOSIS OF PROSTATIC CANCER
J Urol vol 135 pp 951 954 1986

Clements, R , Griffiths, G J and Peeling, W B "STATE OF THE ART" TRANSRECTAL ULTRASOUND IMAGING IN THE ASSESSMENT OF PROSTATIC DISEASE
Br J Radiol vol 64 pp 193 200 1991

Conners, R W and Harlow C A A THEORETICAL COMPARISON OF TEXTURE ALGORITHMS
IEEE Trans Patt Anal Mach Intel vol PAMI-2 pp 204-222 1980

Coplen, D E , Andriole, G L Yuan, J J J and Catalona, W J THE ABILITY OF SYSTEMATIC TRANSRECTAL ULTRASOUND GUIDED BIOPSY TO DETECT PROSTATE CANCER IN MEN WITH THE CLINICAL DIAGNOSIS OF BENIGN PROSTATIC HYPERPLASIA
J Urol vol 146 pp 75 77 1991

Dahnert, W F , Hamper, U M , Eggleston, J C , Walsh, P C and Sanders, R C PROSTATIC EVALUATION BY TRANSRECTAL SONOGRAPHY WITH HISTOPATHOLOGIC CORRELATION THE ECHOPENIC APPEARANCE OF EARLY CARCINOMA
Radiology vol 158 pp 97 102 1986

de la Rosette, J J M C H , Giesen, R J B , Huynen, A L , Aarnink, R G , van Iersel, M P , Debruyne, F M J and Wijkstra, H AUTOMATED ANALYSIS AND INTERPRETATION OF TRANSRECTAL ULTRASONOGRAPHY IMAGES IN PATIENTS WITH PROSTATITIS
Eur Urol vol 27 pp 47 53 1995

de Souza, P TEXTURE RECOGNITION VIA AUTOREGRESSION
Pattern Recognition vol 15 pp 471 475 1982

du Buf, J M H , Kardan, J and Spann, M TEXTURE FEATURE PERFORMANCE FOR IMAGE SEGMENTATION
Pattern Recognition vol 23 pp 291-309 1990

Ellis W J and Brawer, M K THE SIGNIFICANCE OF ISOECHOIC PROSTATIC CARCINOMA
J Urol vol 152 pp 2304 2307 1994

Epstein, J I Carmichael, M J Partin A W and Walsh, P C SMALL HIGH GRADE ADENOCARCINOMA OF THE PROSTATE IN RADICAL PROSTATECTOMY SPECIMENS PERFORMED FOR NONPALPABLE DISEASE PATHOGENETIC AND CLINICAL IMPLICATIONS
J Urol vol 151 pp 1587 1592 1994

Faul P and Altwein, J E SCREENING DES PROSTATAKARZINOMS Springer Berlin 1995

Ferguson J K , Bostwick, D G , Suman, V , Zincke, H and Oesterling J E PROSTATE-SPECIFIC ANTIGEN DETECTED PROSTATE CANCER PATHOLOGICAL CHARACTERISTICS OF ULTRASOUND VISIBLE VERSUS ULTRAOUND INVISIBLE TUMORS
Eur Urol vol 27 pp 8 12 1995

Finette, S , Bleier A and Swindell, W BREAST TISSUE CLASSIFICATION USING DIAGNOSTIC ULTRASOUND AND PATTERN RECOGNITION TECHNIQUES I METHODS OF PATTERN RECOGNITION
Ultrasonic Imaging vol 5 pp 55-70 1983

Galloway, M M TEXTURE ANALYSIS USING GRAY LEVEL RUN LENGTHS
Comp Graph Im Proc vol 4 pp 172 179 1975

Gelfand, S B , Ravishankar, C S and Delp, E J AN ITERATIVE GROWING AND PRUNING ALGORITHM FOR CLASSIFICATION TREE DESIGN
IEEE Trans Patt Anal Mach Intel vol PAMI 13 pp 163-174 1991

Giesen, R J B and Huynen, A L ULTRASONOGRAPHIC TISSUE DISCRIMINATION, AUTOMATIC DETECTION OF PROSTATE CARCINOMA (MASTER THESIS) Dept of computer science, University of Twente, Enschede the Netherlands 1991

Giesen, R J B , Huynen, A L , de la Rosette, J J M C H , Schaafsma, H E van Iersel, M P , Aarnink, R G , Debruyne, F M J and Wijkstra, H THE RELIABILITY OF COMPUTER ANALYSIS OF ULTRASONOGRAPHIC PROSTATE IMAGES, THE INFLUENCE OF INCONSISTENT HISTOPATHOLOGY
Ultrasound Med Biol vol 20 pp 871-876 1994

Giesen, R J B , Huynen, A L , Aarnink, R G , de la Rosette, J J M C H , Debruyne, F M J and Wijkstra, H CONSTRUCTION AND APPLICATION OF A HIERARCHICAL DECISION TREE FOR THE CLASSIFICATION OF ULTRASONOGRAPHIC PROSTATE IMAGES
MBEC Accepted for publication 1995a

Giesen, R J B , Huynen, A L , de la Rosette, J J M C H , Aarnink, R G , Debruyne, F M J and Wijkstra, H ULTRASONIC COMPUTER IMAGING OF THE PROSTATE, CORRELATION BETWEEN LONGITUDINAL AND TRANSVERSE TEXTURE DESCRIPTIONS
EJUS vol 2 pp 145 149 1995b

Giesen, R J B , Huynen, A L Aarnink, R G , de la Rosette, J J M C H , van de Kaa, C , Oosterhof, G O N Debruyne, F M J and Wijkstra, H COMPUTER ANALYSIS OF TRANSRECTAL ULTRASOUND IMAGES OF THE PROSTATE FOR THE DETECTION OF CARCINOMA A PROSPECTIVE STUDY IN RADICAL PROSTATECTOMY SPECIMENS
J Urol vol 154 pp 1397 1400, 1995c

Haddon, J F and Boyce, J F IMAGE SEGMENTATION BY UNIFYING REGION AND BOUNDARY INFORMATION
IEEE Trans Patt Anal Mach Intel vol PAMI-12 pp 929 948 1990

Haralick, R M , Shanmugam, K and Dinstein, I TEXTURAL FEATURES FOR IMAGE CLASSIFICATION
IEEE Trans Sys Man Cyber vol SMC 3 pp 610 621 1973

Haralick, R M STATISTICAL AND STRUCTURAL APPROACHES TO TEXTURE
Proceedings of the IEEE vol 67 pp 786 803 1979

He, D C , Wang L and Guibert, J TEXTURE DISCRIMINATION BASED ON AN OPTIMAL UTILIZATION OF TEXTURE FEATURES
Pattern Recognition vol 21 pp 141 146 1988

Hendrikx A J M van Helvoort van Dommelen, C A M , van Dijk, M A A M , Reijntjes, A G M and Debruyne, F M J ULTRASONIC DETERMINATION OF PROSTATIC VOLUME A CADAVER STUDY
Urology vol 34 pp 123-125 1989

Hendrikx, A J M , de la Rosette, J J M C H , van Helvoort-van Dommelen, C A M , van Dijk M A A M , Semmelink, H Rijntjes, N V M and Debruyne, F M J HISTOLOGICAL ANALYSIS OF ULTRASONIC IMAGES OF THE PROSTATE, AN ACCURATE TECHNIQUE
Ultrasound Med Biol vol 16 pp 667 674 1990

Hill, C R , Bamber J C , Crawford, D C , Lowe, H J and Webb, S WHAT MIGHT ECHOGRAPHY LEARN FROM IMAGE SIENCE?
Ultrasound Med Biol vol 17 pp 559 575 1991

Hodge, K K , McNeal J E Terris, M K and Stamey, T A RANDOM SYSTEMATIC VERSUS DIRECTED ULTRASOUND GUIDED TRANSRECTAL CORE BIOPSIES OF THE PROSTATE
J Urol vol 142 pp 71 75 1989a

Hodge, K K , McNeal, J E and Stamey, T A ULTRASOUND GUIDED TRANSRECTAL CORE BIOPSIES OF THE PALPABLY ABNORMAL PROSTATE
J Urol vol 142 pp 66-70 1989b

Hsiao J Y and Sawchuk A A UNSUPERVISED TEXTURE IMAGE SEGMENTATION USING FEATURE SMOOTHING AND PROBABILISTIC RELAXATION TECHNIQUES
Comp Vis Graph Im Proc vol 48 pp 1-21 1989

Huynen, A L , Giesen R J B , Wijkstra, H , Laduc, R and Debruyne, F M J DIGITAL IMAGE PROCESSING OF ULTRASONOGRAPHIC PROSTATE IMAGES ON BEHALF OF AUTOMATIC CARCINOMA DETECTION
Proceedings of the 6th World Congress in Ultrasound, World Federation of Ultrasound in Medicine and Biology (WFUMB), sept 1-6, Copenhagen vol pp 8225 1991 (Abstract)

Huynen A L , Giesen, R J B , Laduc, R , Debruyne, F M J and Wijkstra, H HIERARCHICAL DECISION TREE FOR THE CLASSIFICATION OF PROSTATE TISSUE
Proceedings of the 14th Annual International Conference of the IEEE Engineering in Medicine and Biology Society (IEEE EMBS), Oct 29- Nov 1, Paris vol pp 2100-2101 1992 (Abstract)

Huynen A L , Giesen R J B de la Rosette, J J M C H Aarnink R G Debruyne, F M J and Wijkstra, H ANALYSIS OF ULTRASONOGRAPHIC PROSTATE IMAGES FOR THE DETECTION OF PROSTATIC CARCINOMA THE AUTOMATED UROLOGIC DIAGNOSTIC EXPERT SYSTEM
Ultrasound Med Biol vol 20 pp 1 10 1994

Keetch, D W , Catalona, W J and Smith, D S SERIAL PROSTATIC BIOPSIES IN MEN WITH PERSISTENTLY ELEVATED SERUM PROSTATE SPECIFIC ANTIGEN VALUES
J Urol vol 151 pp 1571 1574 1994

Lee, F , Gray, J M , McLeary, R D , Meadows, T R , Kumasaka, G H , Borlaza, G S , Straub, W H , Lee F ,Jr Solomon M H , McHugh T A and Wolf, R M TRANSRECTAL ULTRASOUND IN THE DIAGNOSIS OF PROSTATE CANCER LOCATION ECHOGENICITY, HISTOPATHOLOGY, AND STAGING
The prostate vol 7 pp 117-129 1985

Lee, J S J , Haralick, R M and Shapiro, L G MORPHOLOGIC EDGE DETECTION
IEEE Journal of Robotics and Automation vol RA 3 pp 142 156 1987

Lee, F , Torp Pedersen, S T , Siders D B , Littrup, P J and McLeary R D TRANSRECTAL ULTRASOUND IN THE DIAGNOSIS AND STAGING OF PROSTATIC CARCINOMA
Radiology vol 170 pp 609 615 1989a

Lee F Torp-Pedersen, S T and McLeary, R D DIAGNOSIS OF PROSTATE CANCER BY TRANSRECTAL ULTRASOUND
Urol Clin North Am vol 16 pp 663 673 1989b

Lee, F , Torp Pedersen, S T and Siders D B USE OF TRANSRECTAL ULTRASOUND IN DIAGNOSIS, GUIDED BIOPSY, STAGING, AND SCREENING OF PROSTATE CANCER
Supplement to Urology vol 33 pp 7 12 1989c

Loch T Gouge, J O and Bertermann H RECHNERGESTuTZTE REALTIME-FARB SONOGRAPHIE ZUR OBJEKTIVEN BILDANALYSE
Ultraschall in Klinik und Praxis vol 2 pp 242-244 1987

Loch T , Gettys, T , Cochran, J S , Fulgham, P F and Bertermann, H COMPUTER AIDED IMAGE ANALYSIS IN TRANSRECTAL ULTRASOUND OF THE PROSTATE
World J Urol vol 8 pp 150 153 1990

Lowe, B A and Listrom M B INCIDENTAL CARCINOMA OF THE PROSTATE AN ANALYSIS OF THE PREDICTORS OF PROGRESSION
J Urol vol 140 pp 1340-1344 1988

Mebust, W K , Holtgrewe, H L , Cockett, A T K and Peters, P C TRANSURETHRAL PROSTATECTOMY IMMEDIATE AND POSTOPERATIVE COMPLICATIONS A COOPERATIVE STUDY OF 13 PARTICIPATING INSTITUTIONS EVALUATING 3,885 PATIENTS
J Urol vol 141 pp 243 247 1989

Mettlin, C THE STATUS OF PROSTATE CANCER EARLY DETECTION
Cancer vol 72 (suppl) pp 1050 1055 1993

Mettlin, C , Murphy G P , Ray, P S , Shanberg A , Toi A Chesley, A , Babaian, R J Badalament, R , Kane R A and Lee, F AMERICAN CANCER SOCIETY NATIONAL PROSTATE CANCER DETECTION PROJECT RESULTS FROM MULTIPLE EXAMINATIONS USING TRANSRECTAL ULTRASOUND DIGITAL RECTAL EXAMINATION, AND PROSTATE SPECIFIC ANTIGEN
Cancer vol 71 (suppl) pp 891 898 1993

Morris, D T THE CORRECTION OF ULTRASONIC IMAGE ANALYSIS FEATURES FOR THEIR DEPTH DEPENDENCE
Int J Biomed Comput vol 22 pp 143 152 1988

Oosterveld B J , Thijssen, J M and Verhoef, W A TEXTURE OF B MODE ECHOGRAMS 3 D SIMULATIONS AND EXPERIMENTS OF THE EFFECTS OF DIFFRACTION AND SCATERER DENSITY
Ultrasonic Imaging vol 7 pp 142 160 1985

Oosterveld, B J , Thijssen, J M Hartman, P C and Rosenbusch, G J E DETECTION OF DIFFUSE LIVER DISEASE BY QUANTITATIVE ECHOGRAPHY DEPENDENCE ON *A PRIORI* CHOICE OF PARAMETERS
Ultrasound Med Biol vol 19 pp 21 25 1993

Park Y and Sklansky, J AUTOMATED DESIGN OF LINEAR TREE CLASSIFIERS
Pattern Recognition vol 23 pp 1393 1412 1990

Peeling W B and Griffiths G J IMAGING OF THE PROSTATE BY ULTRASOUND
J Urol vol 132 pp 217-224 1984

Prater, J S and Richard, W D SEGMENTING ULTRASOUND IMAGES OF THE PROSTATE USING NEURAL NETWORKS
Ultrasonic Imaging vol 14 pp 159 185 1992

Ragde, H Aldape, H C and Bagley, C M ULTRASOUND GUIDED PROSTATE BIOPSY BIOPTY GUN SUPERIOR TO ASPIRATION
Urology vol 32 pp 503 506 1988

Russell, J M and Resnick, M I ULTRASOUND IN UROLOGY
Urol Clin North Am vol 6 pp 445 468 1979

Scardino, P T EARLY DETECTION OF PROSTATE CANCER
Urol Clin North Am vol 16 pp 635 655 1989

Scardino P T , Shinohara, K , Wheeler, T M and Carter, S St C STAGING OF PROSTATE CANCER, VALUE OF ULTRASONOGRAPHY
Urol Clin North Am vol 16 pp 713 734 1989

Schulze, H BIOLOGY OF PROSTATE CANCER In Altwein, J E , Faul, P and Schneider, W editors INCIDENTAL CARCINOMA OF THE PROSTATE Berlin Springer, 1991 pp 41 45

Schuster, E , Knoflach, P , Huber, K and Grabner, G AN INTERACTIVE PROCESSING SYSTEM FOR ULTRASONIC COMPOUND IMAGING, REAL TIME IMAGE PROCESSING AND TEXTURE ANALYSIS
Ultrasonic Imaging vol 8 pp 131 150 1986

Schuster, E , Knoflach, P , Kratzik, C , Hainz, A and Huber, K OBJEKTIVE GEWEBS DIFFERENZIERUNG IN DER SONOGRAPHIE MIT HILFE DER LOKALEN TEXTURANALYSE
Acta Med Austriaca vol 14 pp 144 148 1987

Schuster, E , Knoflach, P and Grabner, G LOCAL TEXTURE ANALYSIS AN APPROACH TO DIFFERENTIATING LIVER TISSUE OBJECTIVELY
J Clin Ultrasound vol 16 pp 453 461 1988

Sethi, I K and Sarvarayudu, G P R HIERARCHICAL CLASSIFIER DESIGN USING MUTUAL INFORMATION
IEEE Trans Patt Anal Mach Intel vol PAMI 4 pp 441-445 1982

Shinohara, K , Scardino, P T , Carter, S St C and Wheeler, T M PATHOLOGIC BASIS OF THE SONOGRAPHIC APPEARANCE OF THE NORMAL AND MALIGNANT PROSTATE
Urol Clin North Am vol 16 pp 675 691 1989

Thijssen J M , Oosterveld, B J , Hartman, P C and Rosenbusch, G J E CORRELATIONS BETWEEN ACOUSTIC AND TEXTURE PARAMETERS FROM THE RF AND B MODE LIVER ECHOGRAMS
Ultrasound Med Biol vol 19 pp 13 20 1993

van Gool, L Dewaele, P and Oosterlinck, A TEXTURE ANALYSIS ANNO 1983
Comp Vis Graph Im Proc vol 29 pp 336 357 1985

van Vliet, L J ; Young, I T and Beckers, G L A NONLINEAR LAPLACE OPERATOR AS EDGE DETECTOR IN NOISY IMAGES
Comp Vis Graph Im Proc vol 45 pp 167-195 1989

Vistnes, R TEXTURE MODELS AND IMAGE MEASURES FOR TEXTURE DISCRIMINATION
Int J Comp Vision vol 3 pp 313 336 1989

Waag, R C , Demczar, B A and Case, T J NONLINEAR RECEIVER COMPRESSION EFFECTS ON THE AMPLITUDE DISTRIBUTION OF BACKSCATTERED ULTRASONIC SIGNALS
IEEE Trans Biomed Eng vol BME-38 pp 628 633 1991

Wang, L and He, D -C TEXTURE CLASSIFICATION USING TEXTURE SPECTRUM
Pattern Recognition vol 23 pp 905-910 1990

Waterhouse, R L and Resnick, M I THE USE OF TRANSRECTAL PROSTATIC ULTRASONOGRAPHY IN THE EVALUATION OF PATIENTS WITH PROSTATIC CARCINOMA
J Urol vol 141 pp 233-239 1989

Wells, P N T ULTRASONICS IN CLINICAL DIAGNOSIS Churchill Livingstone Edinburgh 1977

Zielke, Th , Nauth, P , Stein, N , von Seelen, W and Loch, E G QUANTITATIVE VERFAHREN BEI DER ULTRASCHALLDIAGNOSTIK
Radiologe vol 25 pp 468-473 1985

Zweig, M H and Campbell, G RECEIVER OPERATING CHARACTERISTIC (ROC) PLOTS A FUNDAMENTAL EVALUATION TOOL IN CLINICAL MEDICINE
Clin Chem vol 39 pp 561-577 1993

PUBLICATIONS

Aarnink, R G , Giesen, R J B **Huynen, A L** , Debruyne F M J and Wijkstra, H AUTOMATED PROSTATE VOLUME DETERMINATION
Proc IEEE 14th Ann Int Conf in Med and Biol vol 5 pp 2146 2147 1992 (Abstract)

Aarnink, R G , **Huynen, A L** , Giesen, R J B , de la Rosette, J J M C H , Debruyne F M J and Wijkstra, H AN EDGE DETECTION SCHEME FOR PROSTATE BOUNDARY DETERMINATION
Proc IEEE 15th Ann Int Conf in Med and Biol vol 1 pp 230-231 1993 (Abstract)

Aarnink, R G , **Huynen, A L.**, Giesen, R J B , de la Rosette, J J M C H , Debruyne, F M J and Wijkstra, H AUTOMATED VOLUME MEASUREMENTS OF THE PROSTATE WITH AUDEX
Journal of EndoUrology vol 7 suppl 1 pp S191, 1993 (Abstract)

Aarnink, R G , **Huynen, A L** , de la Rosette, J J M C H Giesen, R J B , Debruyne, F M J and Wijkstra, H GEAUTOMATISEERDE PROSTAAT VOLUME BEPALING MET AUDEX
Nederlands Tijdschrift voor Geneeskunde vol 36 pp 1851, 1993 (Abstract)

Aarnink, R G , **Huynen, A L** , de la Rosette, J J M C H , Giesen, R J B , Debruyne, F M J and Wijkstra, H AUTOMATED VOLUME DETERMINATION FOR BPH FOLLOW-UP
Proc 2nd Int Congress DUA 1993 pp 89, 1993 (Abstract)

Aarnink, R G , Giesen R J B , **Huynen, A** L , de la Rosette, J J M C H , Debruyne, F M J and Wijkstra H PLANIMETRIC VOLUMETRY OF THE PROSTATE INFLUENCE OF THE STEP SIZE
Proc IEEE 16th Ann Int Conf in Med and Biol vol 1 pp 716-717 1994 (Abstract)

Aarnink, R G Giesen R J B , **Huynen, A L** , de la Rosette, J J M C H Debruyne, F M J and Wijkstra H A PRACTICAL CLINICAL METHOD FOR CONTOUR DETERMINATION IN ULTRASONOGRAPHIC PROSTATE IMAGES
Ultrasound in Med & Biol vol 20 pp 705-717, 1994

Aarnink, R G , de la Rosette, J J M C H , **Huynen, A L** , Giesen, R J B , Debruyne, F M J and Wijkstra H AUTOMATED OBJECTIVE PROSTATE VOLUME DETERMINATION WITH AUDEX
Proc XIth congress of the EAU pp 201, 1994 (Abstract)

Aarnink R G , **Huynen, A L** , Giesen, R J B , de la Rosette, J J M C H , Debruyne, F M J and Wijkstra, H AUTOMATED PROSTATE VOLUME DETERMINATION WITH ULTRASONOGRAPHIC IMAGING
J Urol vol 153 pp 1549 1554, 1995

Aarnink R G , de la Rosette, J J M C H., Giesen, R J B **Huynen, A L** , Debruyne, F M J and Wijkstra, H STANDARDIZED ASSESSMENT TO ENHANCE THE DIAGNOSTIC VALUE OF PROSTATE VOLUME, PART II CORRELATION WITH PSA LEVELS
The prostate, accepted for publication, 1995

Aarnink, R G , de la Rosette, J J M C H , **Huynen, A L** Giesen, R J B , Debruyne, F M J and Wijkstra, H STANDARDIZED ASSESSMENT TO ENHANCE THE DIAGNOSTIC VALUE OF PROSTATE VOLUME, PART I MORPHOMETRY IN PATIENTS WITH LOWER URINARY TRACT SYMPTOMS
The prostate, accpeted for publication, 1995

Aarnink R G , Giesen, R J B de la Rosette, J J M C H , **Huynen, A.L** , Debruyne, F M J , Wijkstra, H PLANIMETRIC VOLUMETRY OF THE PROSTATE HOW ACCURATE IS IT?
Physiological Measurement vol 16 pp 141 150, 1995

Debruyne, F M J , **Huynen, A L** , Giesen, R J B , Aarnink, R G , de la Rosette, J J M C H and Wijkstra, H
AUDEX A COMPUTER SYSTEM FOR THE ANALYSIS OF ULTRASONOGRAPHIC PROSTATE IMAGES
Journal of EndoUrology vol 7 suppl 1 pp S208, 1993 (Abstract)

de la Rosette, J J M C H , Giesen R J B , **Huynen, A L** , Aarnink, R G , Debruyne, F M J and Wijkstra, H
CANCER DETECTION IN THE PROSTATE, THE POSSIBILITIES OF COMPUTER ANALYSIS
Journal of EndoUrology vol 7 suppl 1 pp S200, 1993 (Abstract)

de la Rosette J J M C H , Giesen, R J B , **Huynen, A L** , Aarnink, R G , Debruyne, F M J and Wijkstra, H
COMPUTERIZED ANALYSIS OF TRANSRECTAL ULTRASONOGRAPHY IMAGES IN THE DETECTION OF PROSTATE CARCINOMA
Br J Urol vol 75 pp 485-491 1995

de la Rosette, J J M C H , Giesen, R J B , **Huynen, A.L** , Aarnink, R G , van Iersel, M P , Debruyne, F M J and Wijkstra, H AUTOMATED ANALYSIS AND INTERPRETATION OF TRANSRECTAL ULTRASONOGRAPHY IMAGES IN PATIENTS WITH PROSTATITIS
Eur Urol vol 27 pp 47 53, 1995

Geboers A D H , Giesen, R J B **Huynen, A L** Aarnink, R G , Wijkstra, H and Debruyne, F M J IMAGING IN BPH PATIENTS
Arch Esp de Urol vol 47 (9) pp 857 865 1994

Giesen, R J B and **Huynen, A L** Ultrasonographic tissue discrimination, automatic detection of prostate carcinoma (Master thesis)
Enschede, the Netherlands dept of computer sience, University of Twente, 1991

Giesen R J B , **Huynen, A.L** , Laduc, R , Wijkstra, H and Debruyne, F M J AUDEX AUTOMATED IMAGE ANALYSIS FOR THE DETECTION OF PROSTATE CARCINOMA
Libro de Abstracts,22nd Congress Soc Int D'Urology vol 1991 (Abstract)

Giesen, R J B , **Huynen, A L** , Wijkstra, H , Hendrikx, A J M , Laduc, R and Debruyne, F M J VERWERKING VAN ECHOGRAFIEBEELDEN T B V PROSTAAT KARAKTERISERING
Utrasonoor Bulletin vol 1 pp 15, 1991 (Abstract)

Giesen, R J B , **Huynen, A.L.**, Wijkstra, H , Laduc, R and Debruyne, F M J AUTOMATED PROSTATE CARCINOMA DETECTION WITH THE USE OF TISSUE CHARACTERISATION
Proc 1st Int Congress DUA pp 8, 1991 (Abstract)

Giesen R J B , **Huynen, A L** , Aarnink, R G de la Rosette, J J M C H , Debruyne, F M J and Wijkstra, H
THE USE OF THE AUDEX SYSTEM IN DISCRIMINATION BETWEEN BPH AND CARCINOMA
Proc 2nd Int Congress DUA 1993 pp 88 1993 (Abstract)

Giesen, R J B , **Huynen, A L** , Aarnink, R G , de la Rosette, J J M C H , Debruyne, F M J and Wijkstra, H
WEEFSEL KARAKTERISERING IN ECHOGRAFISCHE PROSTAAT BEELDEN
Utrasonoor Bulletin vol 21-2 pp 35, 1993 (Abstract)

Giesen, R J B , **Huynen, A.L.**, Aarnink R G de la Rosette, J J M C H , Debruyne, F M J and Wijkstra, H
AN APPLICATION OF HIERARCHICAL DECISION TREES FOR THE CLASSIFICATION OF PROSTATE TISSUE
Proc IEEE 15th Ann Int Conf in Med and Biol vol 1 pp 308 309, 1993 (Abstract)

Giesen, R J B , **Huynen, A.L** , Laduc, R , Debruyne, F M J and Wijkstra, H EEN PROSPECTIEVE EVALUATIE VAN HET AUDEX SYSTEEM
Nederlands Tijdschrift voor Geneeskunde vol 137 (3) pp 168, 1993 (Abstract)

Giesen, R.J.B , **Huynen, A.L.**; Laduc, R.; Debruyne, F.M.J and Wijkstra, H A PROSPECTIVE EVALUATION OF THE AUDEX SYSTEM.
J.Urol. vol 4: pp 287A, 1993.(Abstract)

Giesen, R J.B., **Huynen, A.L.**, de la Rosette, J.J.M.C.H ; Aarnink, R.G.; Debruyne, F.M.J and Wijkstra, H. INTERPRETATION OF ULTRASONOGRAPHIC PROSTATE IMAGES WITH THE USE OF COMPUTER ANALYSIS
Proceedings SIU 1994.(Abstract)

Giesen, R.J.B.; **Huynen, A.L.**; de la Rosette, J J.M.C.H., Schaafsma, H.E.; van Iersel, M.P ; Aarnink, R.G.; Debruyne, F M.J. and Wijkstra, H. THE RELIABILITY OF COMPUTER ANALYSIS OF ULTRASONOGRAPHIC PROSTATE IMAGES; THE INFLUENCE OF INCONSISTENT HISTOPATHOLOGY.
Ultrasound in Med.& Biol. vol 20· pp 871-876; 1994

Giesen, R.J B.; **Huynen, A.L.**, Aarnink, R.G., de la Rosette, J.J.M C H ; Debruyne, F.M.J. and Wijkstra, H CONSTRUCTION AND APPLICATION OF A HIEARCHICAL DECISION TREE FOR THE CLASSIFICATION OF ULTRASONOGRAPHIC PROSTATE IMAGES
Med Biol.Eng.Comp. accepted for publication; 1995.

Giesen, R.J B.; **Huynen, A.L.**; Aarnink, R.G ; de la Rosette, J.J.M.C.H., Kaa v d , C.; Oosterhof, G O.N. and Wijkstra, H. COMPUTER ANALYSIS OF TRANSRECTAL ULTRASOUND IMAGES OF THE PROSTATE FOR THE DETECTION OF CARCINOMA· A PROSPECTIVE STUDY IN RADICAL PROSTATECTOMY SPECIMENS.
J Urol. vol 154: pp 1397-1400, 1995.

Giesen, R.J.B., **Huynen, A.L.**; Laduc, R.; Debruyne, F.M.J and Wijkstra, H. THE USE OF THE AUTOMATED UROLOGIC DIAGNOSTIC EXPERT (AUDEX) SYSTEM FOR THE DETECTION OF PROSTATE CARCINOMA
Springer Verlag,Screening des Prostatkarzinoma 1995

Giesen, R.J.B., **Huynen, A.L.**; de la Rosette, J.J.M C.H., Aarnink, R.G.; Debruyne, F.M.J. and Wijkstra, H. ULTRASONIC COMPUTER IMAGING OF THE PROSTATE. CORRELATION BETWEEN LONGITUDINAL AND TRANSVERSE TEXTURE DESCRIPTIONS
European Journal of Ultrasound vol 2 pp 145-149; 1995.

Huynen, A.L.; Giesen, R.J B ; Laduc, R., Wijkstra, H. and Debruyne, F.M.J DIGITAL IMAGE PROCESSING OF ULTRASONOGRAPHIC PROSTATE IMAGES ON BEHALF OF AUTOMATIC CARCINOMA DETECTIONS.
Proc.6th.World.Congress in Ultrasound, WFUMB pp 8225:1991.(Abstract)

Huynen, A.L.; Giesen, R J.B.; Laduc, R.; Debruyne, F.M.J. and Wijkstra, H. THE AUTOMATED UROLOGIC DIAGNOSTIC EXPERT (AUDEX); A SYSTEM FOR COMPUTERIZED VOLUMETRY AND AUTOMATED CARCINOMA DETECTION IN THE PROSTATE.
Proc.1st.Int.Symp. DUST vol 1. pp 8; 1991.(Abstract)

Huynen, A.L., Giesen, R.J.B.; Wijkstra, H., Laduc, R. and Debruyne, F.M.J. STUDY OF THE POSSIBILITIES FOR AUTOMATIC CARCINOMA DETECTION WITH THE USE OF DIGITAL PROCESSING OF ULTRASONOGRAPHIC PROSTATE IMAGES (AUDEX).
Libro de Abstracts,22nd Congress Soc.Int.D'Urology pp 277, 1991.(Abstract)

Huynen, A.L.; Giesen, R.J.B.; Laduc, R., Debruyne, F M.J. and Wijkstra, H. HIERARCHICAL DECISION TREE FOR THE CLASSIFICATION OF PROSTATE TISSUE.
Proc.IEEE 14th Ann.Int.Conf.in Med.and Biol. vol 5: pp 2100-2101; 1992.(Abstract)

Huynen, A L , Giesen, R J B , Wijkstra H , Hendrikx, A J M , Laduc, R and Debruyne, F M J AUTOMATISCHE CARCINOOMHERKENNING IN DE PROSTAAT VOORLOGIPE RESULTATEN
Nederlands Tijdschrift voor Geneeskunde vol 136 (7) pp 346, 1992 (Abstract)

Huynen, A L , Giesen R J B Aarnink, R G , de la Rosette, J J M C H , Debruyne, F M J and Wijkstra H COMPUTER ANALYSIS OF ULTRASONOGRAPHIC PROSTATE IMAGES
Journal of EndoUrology vol 7 suppl 1 pp S191, 1993 (Abstract)

Huynen, A L , Giesen R J B Aarnink, R G , de la Rosette J J M C H , Froeling, F M , Debruyne, F M J and Wijkstra, H COMPUTERIZED INTERPRETATION OF ULTRASONOGRAPHIC PROSTATE IMAGES THE AUTOMATED UROLOGIC DIAGNOSTIC EXPERT SYSTEM
Minimally Invasive Therapy vol 2 suppl 1 pp 90 1993 (Abstract)

Huynen, A L , Giesen R J B Aarnink R G , de la Rosette, J J M C H , Debruyne, F M J and Wijkstra, H PRE AND POSTPROCESSING ALGORITHMS FOR THE CORRECTION OF POSITION DEPENDENCIES OF IMAGE PROCESSING PARAMETERS IN ULTRASONOGRAPHIC PROSTATE IMAGES
Proc IEEE 16th Ann Int Conf in Med and Biol vol 1 pp 666 667, 1994 (Abstract)

Huynen, A L Giesen, R J B , Aarnink, R G , de la Rosette J J M C H , Debruyne F M J and Wijkstra, H PROSTATE TISSUE CHARACTERISATION WITH ULTRASONOGRAPHIC IMAGE ANALYSIS
European Journal of Ultrasound vol 1 suppl 1 pp S5, 1994 (Abstract)

Huynen, A L , Giesen, R J B , de la Rosette, J J M C H , Aarnink, R G , Debruyne, F M J and Wijkstra H ANALYSIS OF ULTRASONOGRAPHIC PROSTATE IMAGES FOR THE DETECTION OF PROSTATE CARCINOMA THE AUTOMATED UROLOGIC DIAGNOSTIC EXPERT SYSTEM
Ultrasound in Med & Biol vol 20 pp 1-10, 1994

Huynen, A L , Giesen, R J B , de la Rosette J J M C H , Aarnink, R G Debruyne F M J and Wijkstra, H GERICHTE PROSTAATBIOPTEN MET BEHULP VAN COMPUTERANALYSE VAN TRANSRECTALE ECHOGRAFISCHE PROSTAATBEELDEN
Nederlands Tijdschrift voor Geneeskunde vol 138 (43) pp 2169, 1994 (Abstract)

Huynen, A.L , Giesen, R J B , Aarnink, R G , de la Rosette, J J M C H , Debruyne, F M J and Wijkstra, H POSITION DEPENDANT ENHANCEMENT OF ULTRASONOGRAPHIC TEXTURAL FEATURES
Ultrasound Med Biol submitted, 1995

Wijkstra H Giesen, R J B , **Huynen, A L** , Laduc, R and Debruyne, F M J AUTOMATIC PROSTATE CARCINOMA DETECTION BY THE USE OF TISSUE CHARACTERISATION
Proc IEEE 13th Ann Int Conf in Med and Biol vol 1 pp 171-172, 1991 (Abstract)

CURRICULUM VITAE

De schrijver van dit proefschrift werd geboren op 10 mei 1967 te Heerlen. Al op jonge leeftijd begon hij zich te interesseren voor de wetenschap. Door het opblazen van zowel een electronische als een chemische experimenteer-doos, werd niet alleen zijn belangstelling voor het onderzoek vergroot, maar besloot hij ook om z'n experimenten en z'n wetenschappelijke carrière op een meer gestructureerde manier aan te pakken.

Hij begon in 1979 aan de middelbare school opleiding aan het Katholiek Gymnasium Rolduc te Kerkrade. Met een ß-vakkenpakket sloot hij deze opleiding af in 1985, waarna hij de informatica opleiding begon te volgen aan de Technische Hogeschool Twente. Na, in het begin van z'n studie, de nodige theoretische kennis opgedaan te hebben, leerde hij al snel de voor- maar vooral de nadelen van het gebruik van computers kennen. Bovendien merkte hij dat hem vooral de praktische toepassingen van deze studie aanspraken en mede daarom besloot hij zich te gaan specialiseren op biomedisch onderzoek De eerste praktijk ervaring kreeg hij d.m.v. een stageperiode aan de vakgroep Medische Informatica en Statistiek van de Rijksuniversiteit Limburg. Tijdens deze periode werden twee programma's ontwikkeld om studenten wegwijs te maken in de medische beslisvorming. Tijdens zijn studie begon zich, d.m.v. zijn hobby fotografie, de interesse te ontwikkelen voor beelden, een ontwikkeling die ook zou doorzetten in zijn wetenschappelijke werk Zijn afstudeeropdracht volbracht hij aan de afdeling Urologie van het Academisch Ziekenhuis Nijmegen. Hier onderzocht hij de mogelijkheden om, m.b.v. een computer, kanker te herkennen in echografische prostaatbeelden. Naar aanleiding van de positieve resultaten van dit onderzoek, werd er een vervolgonderzoek opgestart om de verwachte weefseltypering te realiseren. Dit onderzoek heeft uiteindelijk geleid tot het hier voor U liggende proefschrift.

Stellingen behorende bij het proefschrift

AUTOMATED INTERPRETATION OF ULTRASONOGRAPHIC PROSTATE IMAGES

door A.L. Huynen:

I. Door de evolutie (volgens Darwin) is de menselijke visuele perceptie gespecialiseerd in het schatten van diepte en het herkennen van bewegende voorwerpen. De menselijke waarnemer is daardoor niet in staat alle relevante informatie uit een echobeeld te halen.

II. Interpretatie van echografische prostaatbeelden is subjectief en sterk afhankelijk van de kennis en ervaring van de onderzoeker.

III. D.m.v. automatische analyse van echobeelden van de prostaat is een objectievere interpretatie van deze beelden mogelijk en kan een nauwkeuriger volumebepaling en weefseltypering plaatsvinden.
Dit proefschrift.

IV. Voor de patiënten populatie met prostaatklachten is de kanker detectie met automatische beeldanalyse meer als twee keer zo nauwkeurig als de standaard klinische diagnose.
Dit proefschrift.

V. Met de algoritmen, geoptimaliseerd voor het onderscheiden van maligne en benigne weefsel, is het niet mogelijk een onderscheid te maken tussen benigne weefsel en prostatitis.
Dit proefschrift.

VI. Hoewel de inhomogeniteit van echobeelden terug te vinden is in de textuurkenmerken, heeft dit niet veel invloed op de weefseltypering d.m.v. automatische beeldanalyse.
Dit proefschrift.

VII. De noodzaak voor en de gevolgen van een screeningsprogramma voor prostaatkanker zijn tot op heden nog niet duidelijk. Ook de rol die de verschillende klinisch diagnostische hulpmiddelen daarin kunnen dan wel moeten spelen is nog onderwerp van discussie.

VIII. Het bepalen van 'normaalwaarden' in een gezonde populatie, om drempelwaarden te bepalen voor het detecteren van ziekte, getuigt van slechte kennis over beslisvorming en speltheorie.

IX. In de (medische) wetenschap is er niet altijd een duidelijke grens te leggen tussen het gebruik en misbruik van statistische methoden.

X. Medicine is only slowly reaching the stage at which we recognize how little we know.
David Weatherall: Sience and the quiet art; the role of medical research in medical care.
Nature Medicine vol 1, p.p. 478, 1995

XI. De controle door de promotor op de stellingen bij een proefschrift, beperkt de promovendus aanzienlijk in zijn vrijheid van meningsuiting.